Inorganic Chemistry Communications 145 (2022) 109935

Contents lists available at ScienceDirect

Inorganic Chemistry Communications

journal homepage: www.elsevier.com/locate/inoche

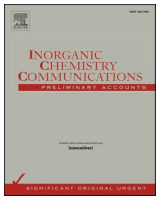

Short communication

Experimental and DFT studies of 2-methyl-quinoxaline and its silver (I) complex: Non-covalent interaction analysis, antimicrobial activity and molecular docking study

Ceyhun Kucuk [a], Senay Yurdakul [a,*], Sibel Celik [b], Belgin Erdem [b]

[a] Department of Physics, Gazi University, Ankara, Turkey
[b] Department of Health Care Services, Ahi Evran University, Kırşehir, Turkey

ARTICLE INFO

Keywords:
2-Methyl-quinoxaline
Silver complex
Vibrational spectra
AIM
Molecular docking
RDG

ABSTRACT

The current study describes the characterization and vibrational spectra (elemental analysis, FT-IR, ^{1}H NMR and UV–Visible absorption) of 2-Methyl-quinoxaline (2-MQ) and synthesized [Ag(2-Methyl-quinoxaline)(NO_3)]. The experimental investigation is supported by theoretical calculations at the DFT level. The frontier molecular orbitals (HOMO and LUMO), the global reactivity descriptors, MEP, and thermodynamic analysis are also computed to investigate the reactivity of the ligand and the complex. The intermolecular interactions in the title compound were analyzed by topological AIM and RDG approaches. The chemical structure of the ligand and its Ag(I) complex were elucidated by the ELF analysis. In addition, a molecular docking study was implemented to look into the studied compounds for their antibacterial activity. According to the molecular docking study used to evaluate the inhibitory effect on target proteins for antimicrobial drugs, the metal complex has a greater binding affinity than the free ligand. These compounds might thus be effective antibacterial candidates. Thus, antimicrobial studies have been performed with 2-MQ and Ag(I) complex against various Gram-positive and Gram-negative bacteria. The 2-MQ proved to be the most active compound in this study and showed the highest antimicrobial activity against S. aureus ATCC 29213, B. cereus 709 Roma, V. anguillarum ATCC 43312 and C. albicans ATCC 90028. Antimicrobial activity against Ag(I) complex, L. monocytogenes, V. anguillarum, A. hydrophila, E. aerogenes, S. dysenteria, B. cereus and C. albicans was determined.

1. Introduction

N-heterocyclic compounds are a class of organic compounds with a wide range of applications, including pharmaceuticals [1-4], pesticides, and natural products [5]. Among the various N-heterocyclic compounds, quinoxalines exhibit a wide range of biological features and therapeutic potential in medical research. Numerous studies have been conducted to determine that quinoxaline derivatives are biologically significant drug candidates due to their antibacterial, antifungal, antiviral, antituberculous, antihypertensive, antiprotozoal, insecticidal, antimalarial, anticonvulsant, antidiabetic, anticancer, kinase inhibitors, antitumor, antiproliferative, and antioxidant properties [6]. The quinoxaline core is an attractive core for obtaining biologically active compounds [7], and drugs containing quinoxaline cores are relatively easy to administer as oral capsules, intramuscular solutions, or rectal suppositories due to their good pharmacokinetic properties [8]. Furthermore, quinoxaline is regarded as a critical nucleus for anticancer drugs [9]. Quinoxaline derivatives are useful in industry because they prevent metal corrosion [10-12], in the synthesis of porphyrins because of their structural similarity to natural chromophores, and in electroluminescent materials [13]. In particular, the quinoxalines, particularly 2-Methyl-quinoxaline derivatives, have been used as antiviral, anticancer, and antibacterial agents in the past [10-12].

Many metals combined with quinoxaline derivatives enable metal chelates to get access to until now unexplored chemical areas in drug development, particularly for designing antimicrobials. Nitrogens with a single electron pair allow 2-Methyl-quinoxaline to complex in coordination chemistry or to function as a protonatable base [13]. Combining bioactive metal ions with pharmacologically active organic ligands is helpful in antimicrobial therapy because it prevents drug resistance, increases activity through synergism, broadens the spectrum of activity, and reduces the number of doses needed. Because of this, the cost of

* Corresponding author.
E-mail address: senayy@gazi.edu.tr (S. Yurdakul).

https://doi.org/10.1016/j.inoche.2022.109935
Received 16 July 2022; Received in revised form 10 August 2022; Accepted 26 August 2022
Available online 31 August 2022

making the drug and the risk of dangerous side effects go down [14]. In previous studies [15], zinc, cadmium, and mercury complexes with 2-Methyl-quinoxaline (2-MQ) were made, their structures were characterized, and thermal and electrical studies were done on them. Silver is a broad-spectrum microbicide and shows high pharmacological activity properties against the difficulties that develop in the treatment of diseases. There is also a great deal of interest in the creation of new silver compounds today. For all these reasons, the Ag (I) complex structure of 2-MQ was synthesized. In our current research, we used elemental analysis, FT-IR, ^{1}H NMR, and UV–Vis spectra to study the structure of the 2-MQ molecule and the its synthesized [Ag(2-MQ)NO_3] compound that was made from it. The density functional theory (DFT) was used to look at the molecular and electronic structures of the compounds in the title. In addition, computational calculations at the level mentioned were done to back up the experimental spectroscopic data of the molecules. The frontier molecular orbital analysis (HOMO-LUMO) was done to figure out the chemical reactivity and molecular electrostatic potential (MEP) surface of the studied title molecule and its synthesized compounds. The AIM and NCI analyses was premeditated for the visual representation of non-covalent chemical bonding. There have also been molecular docking studies to find out how the ligand/complex binds to anti-microbial protein receptors.

2. Material and methods

2.1. Experimental methods

2.1.1. Synthesis of silver complex

Silver nitrate and 2-Methyl-quinoxaline, which were utilized without purification, were purchased by Sigma-Aldrich Chemical Company. The silver complex was created via a chemical synthesize. In 20 mL of ethanol, the ligand (2-MQ) (2 mmol) was liquefied. Then, with steady mixing at 50 °C, $AgNO_3$ (1 mmol) was progressively added to the first produced solution. The finished solution was stored at room temperature for 1 week after 3 h of stirring at the same temperature to allow the solvent to evaporate. The mixture was placed at + 4 °C for 3 months after being wrapped in aluminum foil to prevent exposure to light [16]. The metal-to-ligand ratio in the produced chemical is 1:1. Under ambient conditions, the colorless metal complex was filtered and dried. The yield of the synthesized compound was 76%. For elemental (C, H, and N) analyses, the following calculated and experimental values were reported: [Ag(2-MQ)(NO_3)], CHN Calc: C: 34.42 %, H: 2.56 %, N: 13.38 %. Found: C: 35.32 %, H: 2.48 %, N: 13.20 %.

2.1.2. Instrumentation for recording spectra

The Bruker Vertex 80 FT-IR spectrometer was used to record the infrared spectra of compounds between 4000 and 550 cm^{-1}. The Bruker IFS 66/S system was used to record Far-IR spectra between 700 and 50 cm^{-1}. An Agilent HP 8453 spectrophotometer was used to record UV–Vis spectra in a quartz cell with DMSO as the solvent.

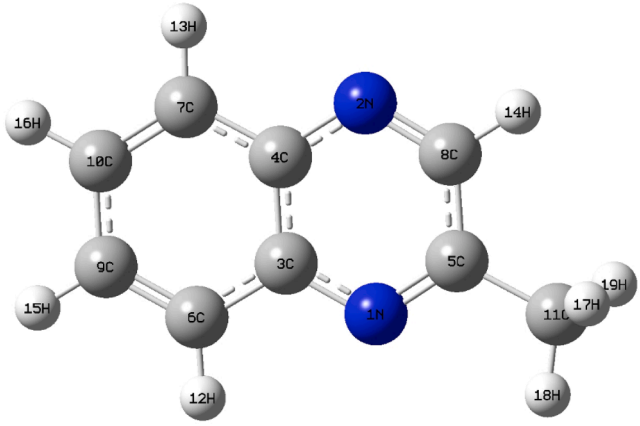

Fig. 1. Optimized molecular structure of 2-MQ.

2.1.3. Microorganisms and conditions for cultivation

S. aureus, S. epidermidis, L. monocytogenes, V. anguillarum, A. hydrophila, E. aerogenes, S. dysenteria, P. aeruginosa, B. cereus, S. typhimurium, E. coli,B. subtilis, K. pneumoniae, E. faecalis and C. albicans were obtained from the American Type Culture Collection. Bacteria and yeast were cultured in Tripticase Soy Broth (TSB) at 37 °C. To make the inoculate, the turbidity of the medium was changed to meet the McFarland Standard, which is 0.5.

2.1.4. Antimicrobial and antiquorum-sensing activities

The antimicrobial activity of 2-Methyl-quinoxaline and its silver (I) complex was determined using the Minimal inhibitory concentration (MIC) and the Agar well diffusion method in this study. The National Committee for Clinical Laboratory Standards (NCCLS) criteria were used to determine the minimum inhibitory concentrations (MIC) of chemicals against bacterial strains [17]. For the MIC test and to culture the bacteria, Mueller-Hinton broth was utilized. Test microorganisms were loaded with nutrient broth (Difco) and overnight at 37 °C for 24–48 h in the agar well diffusion technique.

The Agar well diffusion test and bacterial count (1×10^5 bacteria per mL) on Mueller Hinton Agar (Oxoid) were utilized. A sterile cork borer was used to drill the wells of the culture plates (7 mm in diameter). All the wells were filled with dissolved chemicals containing 10% DMSO (10 mg/mL). The inhibitory zones created on the agar plates were measured in millimeters after 24–48 h (mm). Positive controls included Ampicillin (AMP) (10 μg) and Nystatin (200 μg/ml), whereas negative controls included DMSO. The agar well diffusion test was evaluated using the NCCLS standards [18]. The test was repeated three times, with the average of the results. The diameters of the agar well diffusion regions were evaluated to those of the basic antimicrobials Ampicillin and Nystatin. An antiquorum sensing activity assay on LB agar medium was also done to investigate the compounds' antipathogenic potential. C. violaceum ($1x10^6$) culture was spread on LB agar surface with swap. After that, the chemicals (5 mg/mL) were dissolved in 10% DMSO and poured into the wells. To see if pigment formation was inhibited, samples were incubated h at 30 °C. Because of the prevention of bacterial growth, a distinct halo formation surrounding the wells was judged positive.

2.2. Computational details

2.2.1. Quantum calculation details

The DFT calculations were performed using GAUSSIAN 09 [19]. While the theoretical geometric parameters of 2-MQ were calculated at the DFT/B3LYP level of theory using the 6-311++G (d,p) basis set [20], the geometric parameters of [Ag(2-MQ)(NO_3)] were calculated using the LANL2DZ basis set [21]. HOMO, LUMO, and MEP analyses were visualized using GaussView 5.0 [22]. The UV–vis spectra and features of the optimized structure, such as electronic transitions, excitation energy, absorbances, and oscillator strength, were calculated using time-dependent functional theory (TD-DFT) in DMSO solvent. By employing Multiwfn [23] and the molecular visualization program VMD (Visual Molecular Dynamics) [24], Reduced gradient of density (RDG) analysis leads to an easy-to-catch pictorial visualization of different kinds of non-covalent interactions directly in real space. The Topological data (AIM) were determined using the Multiwfn [22] software. ELF was graphically plotted by the non-covalent interaction (NCI) methods using the Multiwfn program.

2.2.2. Molecular docking procedure

The molecular docking of the chemical compound-proteins binding site was performed using Autodock 2.2.6 software [25]. Before docking,

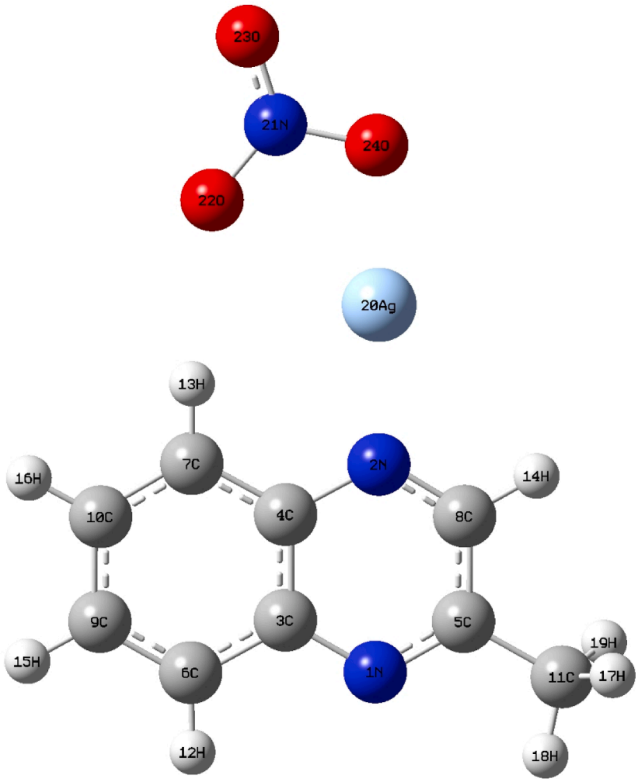

Fig. 2. Optimized molecular structure of [Ag(2-MQ)(NO_3)].

the structure of the protein was cleaned. The active sites of the protein structure were used to create the grid parameter. The binding free energy of the inhibitor (target receptor) in the macromolecule (protein) was evaluated during the docking procedure, as in the work by Abdou et al.[26]. The docked complexes were visualized using Discover Studio Software [27]. The 3D dimensional structure of V. anguillarum, PDB ID: 6AEM and A. hydrophila, PDB ID: 4PJ2 were obtained from the RSCB protein data bank (https://www.pdb.org).

3. Results and discussion

3.1. Molecular structure

The optimized molecular structures of the 2-MQ and [Ag(2-MQ)(NO_3)] complex are shown in Fig. 1 and Fig. 2. The theoretical geometric parameters of the ligand and its Ag(I) complex are given in Table 1. Due to the lack of crystallographic data for the title structures, calculated parameters were compared with X-ray data of 2-Chloro-3-methylquinoxaline [28] and [2-(2-Pyridyl-N)quinoxaline-N] silver(I) nitrate [29]. The bond lengths of all C-C bonds of 2-MQ were found in the range of 1.375–1.504 Å, theoretically. In the benzene ring of 2-MQ ligand, the C_3-C_6, C_4-C_7, and C_9-C_{10} bond lengths are equal to each other, and the calculated value is 1.416 Å. Also, the C_6-C_9 and C_7-C_{10} bond lengths are found to be 1.375 Å. The C_5-C_8 bond length in the pyrazine ring was calculated as 1.431 Å. Also, the N_1-C_3, N_1-C_5, N_2-C_4, and N_2-C_8 bond lengths in the pyrazine ring were calculated as 1.364, 1.314, 1.364, and 1.308 Å, respectively. The calculated C-H bond length values are in the range of 1.083–1.095 Å. To compare the calculated bond lengths and bond angles of 2methylquinoxaline with XRD data of the 2-Chloro-3-methylquinoxaline, root mean square deviation (RMSD) values were calculated. The RMSD value for the bond lengths and angles of 2-Methylquinoxaline was found to be 0.076 and 1.106, respectively. According to these values, the bond lengths and bond angles of 2-Methyl-quinoxaline are in good agreement with the 2-Chloro-3-methylquinoxaline XRD data.

The lengths of the C-C bonds in the [Ag(2-MQ)(NO_3)] complex structure were calculated to be between 1.389 and 1.508. The N_1-C_3, N_1-C_5, N_2-C_4, and N_2-C_8 bond lengths in the pyrazine rings of the complex structure were found to be 1.382, 1.338, 1.392, and 1.338 Å. Also, the C-H bond length values for the silver nitrate complex were calculated in the range of 1.084–1.098 Å. When the C-C, N-C, and C-H bond lengths of the silver nitrate compound were compared with those of 2-Methyl-quinoxaline, it was determined that these values were slightly higher for the complex structure. The N_2-Ag_{20}, Ag_{20}-O_{22}, and Ag_{20}-O_{24} bond lengths were found to be 2.175, 2.637, and 2.178 Å. The N_{21}-O_{22}, N_{21}-O_{23}, and N_{21}-O_{24} bond lengths in the nitrate group are calculated as 1.313,1.265, and 1.362 Å, respectively. Also, bond lengths were compared with the XRD data of [2-(2-Pyridyl-N)quinoxaline-N]silver(I) nitrate and it was determined that they had small differences between each other. The RMSD values for the bond lengths and bond angles of the Ag(I) complex structure were found to be 0.087 and 0.889, respectively.

3.2. Vibrational analysis

The some scaled theoretical wavenumbers and recorded FT-IR and FT-Ra bands with TED analysis of free ligand and its Ag(I) complex are shown in Tables 2 and 3, and experimental Far-IR, FT-IR, and FT-Ra spectra are also shown in Figs. 3–5. In addition, the data outside the selected frequency values for both compounds is given in supplementary Table S1 and Table S2. The calculated frequency values are scaled with a scale factor to be compatible with experimental values. For 2-MQ, a scale factor of 0.983 was used for wavenumbers under 1800 cm^{-1} [30], while 0.9614 was used for wavenumbers over 1800 cm^{-1} [31]. A scale factor of 0.9614 was used in all wavenumbers for [Ag(2-MQ)(NO_3)] [32].

3.2.1. C-H vibration

The C-H stretching vibrations of aromatic structures are observed in the region of 3100–3000 cm^{-1} [33]. Also, the C–H stretching vibrations of methyl (CH_3) groups are found in between 2800 and 3000 cm^{-1} [34]. In the present study, The C-H symmetric and asymmetric vibrations in the benzene ring of 2-Methyl-quinoxaline were calculated at 3074, 3069, 3057, 3046 cm^{-1}. These modes were experimentally observed at 3082 cm^{-1} (s, Ra) and 3060 cm^{-1} (vw, IR). The C-H symmetric and asymmetric stretching vibrations of methyl group were calculated at 3013, 3012, 2957, and 2910 cm^{-1} and observed at 3014 (vw, IR), 2952 (s, Ra), and 2919 (vw, IR)/2917 (s, Ra) cm^{-1}. The C-H stretching vibrations in the aromatic rings of the Ag(I) complex were calculated at 3120, 3108, 3107, 3091, and 3076 cm^{-1}, but they were observed in the FT-Ra spectrum at 3064 cm^{-1} (vw).The modes for the CH3 group of complex structrues were theoretically found to be 3056, 2997, and 2929 cm-1 and were observed at 3053 cm-1 (vw, IR) in the FT-IR spectrum. These stretching vibrations for aromatic rings of 2-quinoxaline carboxylic acid are calculated at 2981, 2975, 2971, 2964, and 2953 cm-1 and observed at 3070, 3050, 2960, and 2920 cm-1 in the FT-IR spectrum [35]. In studies of 7-methoxy-4-methylcoumarin that looked at frequency analysis, the C–H stretching vibrations of the methyl group were found to be 2902 and 2855 cm^{-1} in the FT-IR spectrum [34].

3.2.2. C–H in-plane and out-of-plane bending vibrations

In aromatic compounds, the in-plane C-H bending vibrations are observed in the region of 1300–1000 cm^{-1} [36]. The C-H in-plane bending vibrations for 2-MQ were calculated at 1300, 1274, 1217, 1204, 1136, and 1125 cm^{-1}, and were observed at 1314 (s, IR)/1296 (m/Ra), 1287 (s, IR)/1262 (s, Ra), 1199 (s, IR)/1202 (vw, Ra), 1119 (s, IR) cm^{-1}. For the silver nitrate complex with 2-MQ, these modes were calculated at 1277, 1267, 1205, 1193, 1145, and 1110, while the C-H in-plane bending modes were observed at 1279 (vs, IR)/1263 (m, Ra), 1252 (m, Ra), 1207 (s, IR), 1190 (vw, Ra), and 1162 (w, Ra) cm^{-1} in the vibrational spectra. While the in-plane C-H bending vibrations in the rings of 7-methoxy-4-methylcoumarin were observed at 1347, 1265,

Table 1
Optimized geometrical parameters and of 2-MQ and [Ag(2-MQ)(NO_3)].

Bond Lengths (Å)					Bond Angles (°)				
Parameters	*Calc.	XRD[a]	**Cal.	XRD[b]	Parameters	*Calc.	XRD[a]	**Calc.	XRD[b]
N_1-C_3	1.364	1.374	1.382	1.357	C_3-N_1-C_5	117.50	118.27	118.47	118.30
N_1-C_5	1.314	1.316	1.338	1.314	C_4-N_2-C_8	116.67	116.20	118.74	118.03
N_2-C_4	1.364	1.378	1.392	1.365	N_1-C_3-C_4	121.09	121.37	121.49	120.47
N_2-C_8	1.308	1.297	1.338	1.299	N_1-C_3-C_6	119.63	119.38	119.24	120.24
C_3-C_4	1.425	1.414	1.441	1.425	C_4-C_3-C_6	119.28	119.25	119.26	119.26
C_3-C_6	1.416	1.416	1.424	1.411	N_2-C_4-C_3	120.58	120.12	118.59	119.89
C_4-C_7	1.416	1.413	1.423	1.406	N_2-C_4-C_7	119.82	119.77	121.31	121.11
C_5-C_8	1.431	1.436	1.437	1.424	C_3-C_4-C_7	119.60	120.11	120.09	118.94
C_5-C_{11}	1.504	1.507	1.508	1.495	N_1-C_5-C_8	120.82	118.87	120.51	120.86
C_6-C_9	1.375	1.368	1.389	1.362	N_1-C_5-C_{11}	118.97	119.21	119.13	118.08
C_6-H_{12}	1.084	0.950	1.085	0.929	C_8-C_5-C_{11}	120.21	121.91	120.35	121.05
C_7-C_{10}	1.375	1.373	1.390	1.364	C_3-C_6-C_9	119.96	119.78	119.84	120.18
C_7-H_{13}	1.083	0.950	1.088	0.931	C_3-C_6-H_{12}	118.08	120.11	117.88	119.94
C_8-H_{14}	1.088	–	1.084	0.929	C_9-C_6-H_{12}	121.96	120.11	122.28	119.87
C_9-C_{10}	1.416	1.415	1.428	1.399	C_4-C_7-C_{10}	119.91	119.46	119.27	119.99
C_9-H_{15}	1.084	0.950	1.086	0.930	C_4-C_7-H_{13}	118.06	119.47	120.08	119.92
C_{10}-H_{16}	1.084	0.950	1.086	0.931	C_{10}-C_7-H_{13}	122.02	120.27	120.64	120.08
C_{11}-H_{17}	1.095	0.980	1.098	–	N_2-C_8-C_5	123.34	121.16	122.19	122.36
C_{11}-H_{18}	1.089	0.980	1.092	–	N_2-C_8-H_{14}	117.14	–	117.81	–
C_{11}-H_{19}	1.095	0.980	1.098	–	C_5-C_8-H_{14}	119.52	–	120.00	–
N_2-Ag_{20}	–	–	2.175	–	C_6-C_9-C_{10}	120.71	120.82	120.59	120.32
Ag_{20}-O_{22}	–	–	2.637	–	C_6-C_9-H_{15}	119.93	119.59	120.06	119.81
Ag_{20}-O_{24}	–	–	2.178	–	C_{10}-C_9-H_{15}	119.35	119.58	119.35	119.86
N_{21}- O_{22}	–	–	1.313	1.232	C_7-C_{10}-C_9	120.54	120.57	120.94	121.27
N_{21}- O_{23}	–	–	1.265	1.226	C_7-C_{10}-H_{16}	120.03	119.71	119.46	119.36
N_{21}- O_{24}	–	–	1.362	1.226	C_9-C_{10}-H_{16}	119.42	119.71	119.60	119.36
RMSD	0.076				C_5-C_{11}-H_{17}	110.99	109.47	111.27	–
			0.087						
					C_5-C_{11}-H_{18}	109.76	109.45	109.42	–
					C_5-C_{11}-H_{19}	110.99	109.45	111.26	–
					H_{17}-C_{11}-H_{18}	108.89	109.48	108.70	–
					H_{17}-C_{11}-H_{19}	107.21	109.48	107.41	–
					H_{18}-C_{11}-H_{19}	108.90	109.47	108.70	–
					C_4-N_2-Ag_{20}	–		118.59	–
					N_2-Ag_{20}-O_{22}	–		123.67	–
					O_{22}-Ag_{20}-O_{24}	–		53.39	–
					O_{22}-N_{21}-O_{23}	–		123.79	–
					O_{22}-N_{21}-O_{24}	–		116.45	–
					O_{23}-N_{21}-O_{24}	–		119.75	–
					Ag_{20}-O_{22}-N_{21}	–		84.44	–
					Ag_{20}-O_{24}-N_{21}	–		103.71	–
					RMSD	1.106		0.889	

*2-MQ.
**[Ag(2-MQ)(NO_3)].
[a] XRD parameters of 2-Chloro-3-methylquinoxaline [28].
[b] XRD parameters of 2-(2-Pyridyl-N)quinoxaline-N_1]silver(I) nitrate [29].

1237, and 1110 cm^{-1} in the FT-IR spectrum and observed at 1350 and 1237 cm^{-1} in the FT-Ra spectrum, the out-of-plane C-H vibration bands were observed at 852, 807, 709, 674, and 634 cm^{-1} in the FT-IR spectrum and were observed at 714 cm^{-1} and 677 cm^{-1} in the FT-Ra spectrum [34].

The methyl group contains symmetric and asymmetric C-H in-plane and out-of-plane bending vibrations. These modes were calculated for 2-MQ at 1476, 1458, 1451, 1415, and 1383 cm^{-1} and for [Ag(2-MQ)(NO_3] at 1470, 1452, 1446, 1437, and 1392 cm^{-1}. Also, these modes were observed at 1460 (m, Ra), 1450c (m, Ra), 1407 (w, IR), and 1382 (v, Ra) cm^{-1} for 2-Methyl-quinoxaline and were observed at 1467 (m, IR) and 1472 (m, Ra) cm^{-1} for the title complex. The asymmetric bending vibrations for 7-methoxy-4-methylcoumarin were observed at 1456 and 1441 cm^{-1} in the FT-IR spectrum and were calculated at 1455 and 1444 cm^{-1}, while the symmetric bending vibration was observed at 1422, 1384, and 1376 cm^{-1} in the FT-IR and FT-Ra spectra and calculated at 1428 and 1370 cm^{-1} [34].

While the in-plane rocking vibration that occurred in the methyl group was theoretically calculated at 1018, 1008, and 958 cm^{-1} for free ligand, the out-of-plane rocking vibrations were calculated at 1038 cm^{-1}. Also, these modes were observed at 1032 (w/IR), 1007 (m/IR)/ 993 (vs/Ra), 960 (s, IR)/964 (w, Ra) cm^{-1}. For silever nitrate complex of 2-MQ, the in-plane rocking vibration was calculated at 1007, 996, and 954 cm^{-1}, while the out-of-plane rocking vibration values were calculated at 1047 cm^{-1}. These in-plane and out-plane rocking vibrations were observed at 1028 (s, IR)/1020 (vw, Ra) and 986 (vw, Ra) cm^{-1}, respectively. The in-plane-rocking vibrations of the CH3 group for 7-methoxy-4-methylcoumarin were observed in the FT-IR spectrum at 1153 and 1038 cm^{-1}, and in the FT-Ra spectrum at 1163 cm^{-1}. These vibration modes were calculated at 1159 and 1024 cm^{-1}. Also, the out-of-plane rocking vibrations of 7-methoxy-4-methylcoumarin were calculated to be 1129 and 988 cm^{-1}, and they were seen to be 1134, 979, and 987 cm^{-1} in the FT-IR and FT-Ra spectra [34].

3.2.3. *C–C and C=C stretching vibrations*

The C–C and C=C stretching vibrations in the aromatic molecule rings are generally assigned in the range of 1650–1200 cm^{-1} [37]. The C-C and C=C stretching vibrations of 2-MQ in this region, were theoretically found to be 1648, 1589, 1571, 1502, 1476, 1415, 1362, 1346, 1300, 1274,1217, and 1204 cm^{-1}. Experimental wavenumbers corresponding to these theoretical values were observed at 1612 (vw, IR), 1578 (vw, IR)/ 1597 (s, Ra), 1366 (m, IR), 1344 (vw, Ra), 1314 (s, IR)/

Table 2
Selected vibrational wave numbers at DFT/B3LYP/6–311++G(d,p) basis set, observed IR and Raman frequencies, and their assignments with potential energy distribution (%) for 2-MQ.

Calculated					Observed		
Mode	Fre	Fre[a]	I_{IR}[b]	I_{RA}[b]	IR	Raman	TED[c]
21	975	958	25.47	3.34	960 s	964 w	$14\delta_{CCC}$ + $12\delta_{CCN}$ + $27\delta_{CCH}$
24	1025	1008	18.17	6.78	1007 m	993 vs	$21\upsilon_{CC}$ + $33\delta_{CCH}$
25	1036	1018	4.04	20.42	–	–	$21\upsilon_{CC}$ + $38\delta_{CCH}$
26	1056	1038	2.52	0.16	1032 w	–	$10\gamma_{CCH}$ + $27\Gamma_{CCCH}$ + $15\Gamma_{CNCC}$ + $12\Gamma_{NCCH}$
27	1144	1125	10.36	1.44	1119 s		$16\upsilon_{CC}$ + $12\delta_{CCC}$ + $50\delta_{CCH}$
28	1156	1136	9.87	3.13	–	–	$18\upsilon_{CC}$ + $12\upsilon_{CN}$ + $53\delta_{CCH}$
29	1225	1204	14.91	4.29	1199 s	1202vw	$17\upsilon_{CC}$ + $10\upsilon_{CN}$ + $42\delta_{CCH}$
30	1238	1217	1.23	8.99	–	–	$11\upsilon_{CC}$ + $12\upsilon_{CN}$ + $15\delta_{CCC}$ + $42\delta_{CCH}$
31	1296	1274	5.03	0.41	1287 s	1262 s	$11\upsilon_{CC}$ + $12\upsilon_{CN}$ + $17\delta_{CCH}$ + $11\delta_{CCH}$
32	1322	1300	28.49	1.44	1314 s	1296 m	$25\upsilon_{CC}$ + $15\upsilon_{CN}$ + $17\delta_{CCH}$ + $11\delta_{CCH}$
33	1369	1346	0.51	2.08	–	1344 vw	$14\upsilon_{CC}$ + $13\upsilon_{CN}$ + $38\delta_{CCH}$
34	1386	1362	7.14	100.00	1366 m	–	$30\upsilon_{CC}$ + $12\upsilon_{CN}$ + $28\delta_{CCH}$
35	1407	1383	8.94	9.66	–	1382 vw	$39\delta_{CCH}$ + $35\delta_{HCH}$
36	1439	1415	12.80	60.36	1407 w		$19\upsilon_{CC}$ + $29\upsilon_{CCH}$
37	1476	1451	16.46	34.38	–	1450 m	$23\delta_{CCH}$ + $28\delta_{HCH}$ + $15\Gamma_{CCCH}$ + $15\Gamma_{NCCH}$
38	1483	1458	10.99	6.11	–	1460 m	$36\gamma_{HCH}$ + $25\Gamma_{CCCH}$ + $25\Gamma_{NCCH}$
39	1502	1476	0.77	1.96	–	–	$15\upsilon_{CC}$ + $36\upsilon_{CCH}$ + $10\delta_{CCN}$
40	1528	1502	37.66	3.53	–	–	$25\upsilon_{CC}$ + $10\upsilon_{CN}$ + $44\delta_{CCH}$
41	1598	1571	11.89	10.87	–	–	$28\upsilon_{CC}$ + $10\delta_{CCC}$ + $28\delta_{CCH}$ + $10\delta_{CCN}$
42	1616	1589	22.24	17.83	1578 vw	1597 s	$17\upsilon_{CC}$ + $23\upsilon_{CN}$ + $10\delta_{CCC}$ + $22\delta_{CCH}$ + $14\delta_{CCN}$
43	1653	1648	1.45	4.17	1612 vw	–	$26\upsilon_{CC}$ + $13\delta_{CCC}$ + $45\delta_{CCH}$
44	3027	2910	19.33	43.44	2919 vw	2917 s	$89\upsilon_{CH}$ (sym, CH_3)
45	3076	2957	15.80	13.44	–	2952 s	$77\upsilon_{CH}$ (asym, CH_3)
46	3133	3012	23.85	14.17	–	–	$79\upsilon_{CH}$ (asym, CH_3)
47	3134	3013	15.03	12.34	3014 vw	–	$81\upsilon_{CH}$ (asym, CH_3)
48	3168	3046	2.43	5.79	–	–	$81\upsilon_{CH}$ (asym)
49	3180	3057	7.48	14.28	3060 vw	–	$83\upsilon_{CH}$ (asym)
50	3192	3069	13.24	4.39	–	–	$82\upsilon_{CH}$ (asym)
51	3197	3074	15.52	34.90	–	3082 s	$86\upsilon_{CH}$ (sym)

υ: stretching, δ: in-plane bending, γ: out-plane bending, Γ: torsion, s: strong, m: medium, w: weak, v: very.

[a] Scaled wavenumbers calculated at B3LYP/6-311++G(d,p) using scaling factors 0.983 for the wavenumber less than 1800 cm^{-1} [30] and 0.9614 above 1800 cm^{-1} [31].

[b] Relative absorption intensities and relative Raman intensities normalized with highest peak absorption equal to 100.

[c] Total energy distribution level (TED) less than 10% are not shown.

1296 (m, Ra), 1287 (s, IR)/ 1262 (s, Ra), and 1199 (s, IR)/ 1202 (vw, Ra) cm^{-1}. The C-C and C=C stretching vibrations for the [Ag(2-MQ)(NO_3)] complex structure were calculated at 1593, 1545, 1525, 1470, 1446, 1392, 1391, 1358, 1311, 1277, 1267, and 1205 cm^{-1} and observed at 1611 (vw, IR)/1596 (s, Ra), 1551 (s, Ra), 1467 (m, IR)/ 1472 cm^{-1} (m, Ra), 1279 (vs, IR)/ 1263 (m, Ra), 1252 (m, Ra), and 1207 (s, IR) cm^{-1} in the FT-IR and FT-Ra spectra. These stretching vibrations of 2-quinoxaline carboxylic acid were observed at 1710, 1610, 1460, 1410, and 993 cm^{-1} in the IR and Raman spectrum and were observed at 1020, and 920 cm^{-1} in the IR spectrum [35].

3.2.4. C-N stretching vibrations

The determining of the C-N stretching vibration is difficult due to the several bands that are possibly superimposed in this region. The C-N stretching vibrations are assigned to the 1342–1266 cm^{-1} region [38]. The C-N stretching vibration modes for 2-MQ were observed at 1366 (m, IR), 1344 (vw, Ra), 1314 (s, IR)/ 1296 (m, Ra), and 1287 (w, IR)/ 1262 (m, Ra) $cm^{-1}$and calculated 1362, 1346, 1300 and 1274 cm^{-1}. For silver nitrate complex of 2-Methyl-quinoxaline, these modes were observed 1252 (m, Ra), 1207 (s, IR), 1190 (vw, Ra), and 1162 (w, Ra) cm^{-1} and calculated 1311, 1267, 1205, 1193, and 1145 cm^{-1}. The C-N stretching modes of 2-quinoxaline carboxylic acid were observed at 575 cm^{-1} in the FT-IR spectrum and at 1540 cm^{-1} in both the FT-IR and FT-Ra spectrum. Also, the theoretically computed wavenumbers puted values of the corresponding C-N stretching vibrations were calculated at 1563 and 1537 cm^{-1} [35].

3.2.5. N-O Stretching vibrations

Due to the asymmetric stretching of the nitrate group (NO_3), the IR spectra of the nitrate complexes revealed the characteristic IR frequency for the uncoordinated nitrate group by the emergence of a prominent band near the 1330 cm^{-1} region [39]. This band in the [Ag(2-MQ)(NO3)] complex structure was observed at 1389 (s, Ra)/ 1387 (vs, Ra) cm^{-1} while the band was computed at 1371 cm^{-1}. Also, the N-O stretching vibration values were calculated at 1118 and 899 cm^{-1} and were observed 1135 (m, IR)/ 1139 (w, Ra) and 919 (m, IR)/ 890 (vw, Ra) cm^{-1}. In the literatüre, these vibration of silver(I) nitrate complex with nicotinaldehyde [Ag(3-Py-CHO)$_2$$NO_3$] was observed at 1347 cm^{-1} and calculated at 1363 cm^{-1} [16]. In another study conducted by Bilkan et al. in 2016, N-O stretching vibrations for [$C_{10}H_9N_3$]4$AgNO_3$] were calculated at 1325, 1168, and 934 cm^{-1}, while these vibration values were measured at 1337 (FT-IR)/1334 (FT-Ra) cm-1, 1196 (FT-IR)/1204 (FT-Ra), and 954 (FT-IR) cm^{-1} [40].

3.2.6. Ag-O and Ag-N stretching vibrations

In theory, the symmetric and asymmetric mode values of Ag–O in the IR spectrum are expected to be around 640 cm^{-1}. These stretching

Table 3
Selected vibrational wave numbers at DFT/B3LYP/LANL2DZ basis set, observed IR and Raman frequencies, and their assignments with potential energy distribution (%) for [Ag(2-MQ)(NO_3)].

Calculated					Observed		
Mode	Fre	Fre[a]	I^b_{IR}	I^b_{RA}	IR	Raman	TED[c]
6	105	101	0.55	6.51	100w	–	$10\upsilon_{AgO} + 32\delta_{CNAg} + 13\delta_{AgON} 11\Gamma_{NAgOH}$
8	131	126	1.23	3.85	124vw	123 m	$17\upsilon_{AgO} + 16\delta_{CNAg} + 17\Gamma_{NAgOH}$
10	144	138	0.38	1.93	141vw	–	$32\upsilon_{AgN} + 14\upsilon_{AgO} + 17\delta_{CCN}$
12	272	261	0.60	0.59	–	–	$17\upsilon_{AgO} + 12\delta_{CCC} + 10\delta_{CCN} + 13\delta_{CCH}$
13	298	286	6.42	0.78	–	271w	$32\upsilon_{AgN} + 14\upsilon_{AgO} + 10\delta_{CCC} + 14\delta_{CCN}$
26	740	711	0.74	1.86	719 m	704vw	$10\upsilon_{AgN} + 16\upsilon_{CC} + 14\delta_{CCC} + 14\delta_{CCN} + 14\delta_{CCH}$
32	936	899	14.52	5.82	919 m	890vw	$56\upsilon_{NO} + 19\delta_{ONO}$
34	993	954	3.92	0.05	–	953vw	$15\upsilon_{CC} + 12\delta_{CCC} + 14\delta_{CCN} + 25\delta_{CCH}$
36	1036	996	2.15	1.38	–	986vw	$18\upsilon_{CC} + 33\delta_{CCH} + 10\Gamma_{CCCH} + 10\Gamma_{NCCH}$
37	1048	1007	0.31	3.03	–	–	$17\upsilon_{CC} + 35\delta_{CCH}$
39	1089	1047	1.14	0.18	1028 s	1020vw	$20\gamma_{CCH} + 22\Gamma_{CCCH} + 14\Gamma_{CNCC} + 11\Gamma_{NCCH}$
40	1155	1110	0.74	0.50	–	–	$17\upsilon_{CC} + 13\delta_{CCC} + 40\delta_{CCH}$
41	1163	1118	57.72	0.75	1135 s	1139w	$26\upsilon_{NO} + 26\delta_{ONO}$
42	1191	1145	2.33	0.36	–	1162w	$15\upsilon_{CC} + 13\upsilon_{CN} + 44\delta_{CCH}$
43	1241	1193	0.08	0.68	–	1190vw	$10\upsilon_{CC} + 10\upsilon_{CN} + 11\delta_{CCC} + 41\delta_{CCH}$
44	1254	1205	3.34	0.54	1207 s	–	$18\upsilon_{CC} + 11\upsilon_{CN} + 11\delta_{CCC} + 39\delta_{CCH}$
45	1318	1267	3.51	3.65	–	1252 m	$14\upsilon_{CC} + 14\upsilon_{CN} + 11\delta_{CCN} + 37\delta_{CCH}$
46	1329	1277	0.74	0.37	1279vs	1263 m	$13\upsilon_{CC} + 16\delta_{CCN} + 32\delta_{CCH}$
47	1364	1311	1.97	0.40	–	–	$13\upsilon_{CC} + 14\upsilon_{CN} + 32\delta_{CCH}$
48	1413	1358	6.06	10.20	–	–	$32\upsilon_{CC} + + 32\delta_{CCH}$
49	1427	1371	100.00	1.41	1389 s	1387vs	$34\upsilon_{NO} + 22\delta_{ONO}$
50	1447	1391	4.26	3.19	–	–	$13\upsilon_{CC} + 41\delta_{CCH} + 41\delta_{HCH}$
51	1449	1392	1.33	1.87	–	–	$15\upsilon_{CC} + 36\delta_{CCH} + 10\delta_{HCH}$
52	1495	1437	2.07	5.34	–	–	$36\delta_{CCH} + 10\delta_{HCH} + 11\Gamma_{CCCH} + 11\Gamma_{NCCH}$
53	1505	1446	0.00	0.53	–	–	$12\upsilon_{CC} + 29\delta_{CCH} + 16\delta_{HCH}$
54	1511	1452	3.90	1.19	–	–	$10\delta_{CCH} + 35\gamma_{HCH} + 26\Gamma_{CCCH} + 25\Gamma_{NCCH}$
55	1530	1470	11.01	0.70	1467 m	1472 m	$15\upsilon_{CC} + 36\delta_{CCH} + 11\delta_{HCH}$
56	1587	1525	7.45	1.30	–	–	$20\upsilon_{CC} + 16\upsilon_{CN} + 10\delta_{CCC} + 12\delta_{CCN} + 26\delta_{CCH}$
57	1608	1545	1.19	4.65	–	1551 s	$25\upsilon_{CC} + 13\upsilon_{CN} + 10\delta_{CCC} + 12\delta_{CCN} + 22\delta_{CCH}$
58	1658	1593	0.23	0.53	1611vw	1596 s	$28\upsilon_{CC} + 14\delta_{CCC} + 39\delta_{CCH}$
59	3048	2929	2.32	4.84	–	–	$90\upsilon_{CH}$ (sym, CH_3)
60	3119	2997	3.28	1.43	–	–	$78\upsilon_{CH}$ (asym, CH_3)
61	3180	3056	1.29	0.92	3053vw	–	$78\upsilon_{CH}$ (asym, CH_3)
62	3201	3076	1.88	1.55	–	3064vw	$78\upsilon_{CH}$ (asym)
63	3216	3091	0.50	0.98	–	–	$81\upsilon_{CH}$ (asym)
64	3233	3107	0.77	1.46	–	–	$81\upsilon_{CH}$ (asym)
65	3234	3108	0.51	0.72	–	–	$72\upsilon_{CH}$ (asym)
66	3247	3120	2.79	3.45	–	–	$85\upsilon_{CH}$ (sym)

υ: stretching, δ: in-plane bending, γ: out-plane bending, Γ: torsion, s: strong, m: medium, w: weak, v: very.
aScaled wavenumbers calculated at B3LYP/LANL2DZ using scaling factors 0.961 for all wavenumbers [32].
bRelative absorption intensities and relative Raman intensities normalized with highest peak absorption equal to 100.
cTotal energy distribution level (TED) less than 10% are not shown.

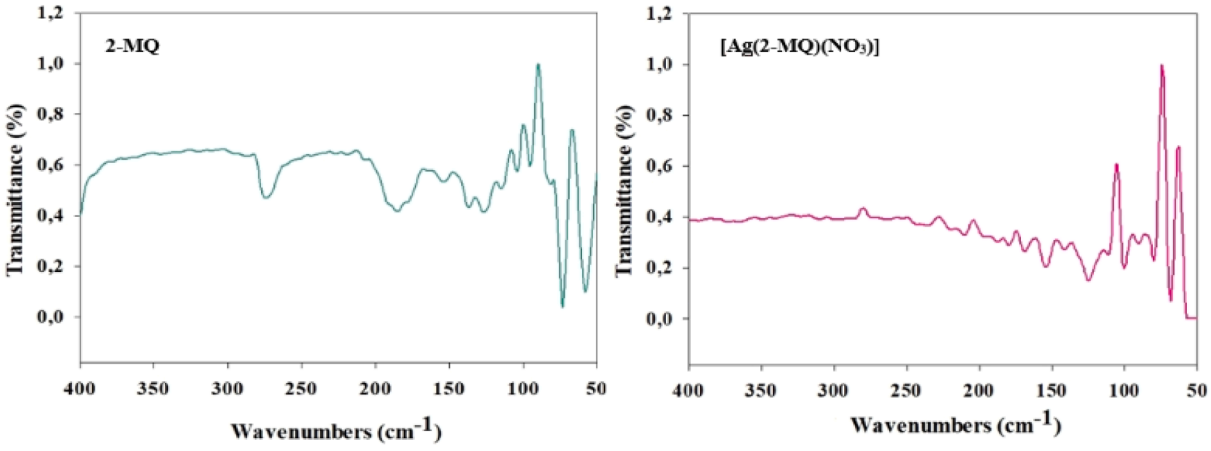

Fig. 3. Experimental Far-IR spectra of 2-MQ and [Ag(2-MQ)(NO_3)].

vibrations of the synthesized silver nitrate complex were measured at 640 (vw, IR)/ 643 (w, Ra) and 124 (vw/IR)/ 123 (m,Ra), and 100 (w, IR) cm^{-1} and were calculated 649, 261, 126, and 101 cm^{-1}. For the [Ag(3-Py-CHO)$_2$NO3] complex structure, the Ag-O stretching vibration was observed in the IR spectrum at 642 cm^{-1} in the literature [16]. The Ag-N stretching vibrations of [Ag(2-MQ)(NO3)] complex were observed at 719 (m, IR)/ 704 (vw, Ra), 271 (w, Ra), and 141 (vw, IR) cm^{-1} and were computed 711, 286, and 138 cm^{-1}. In the literature, the Ag(I)-N

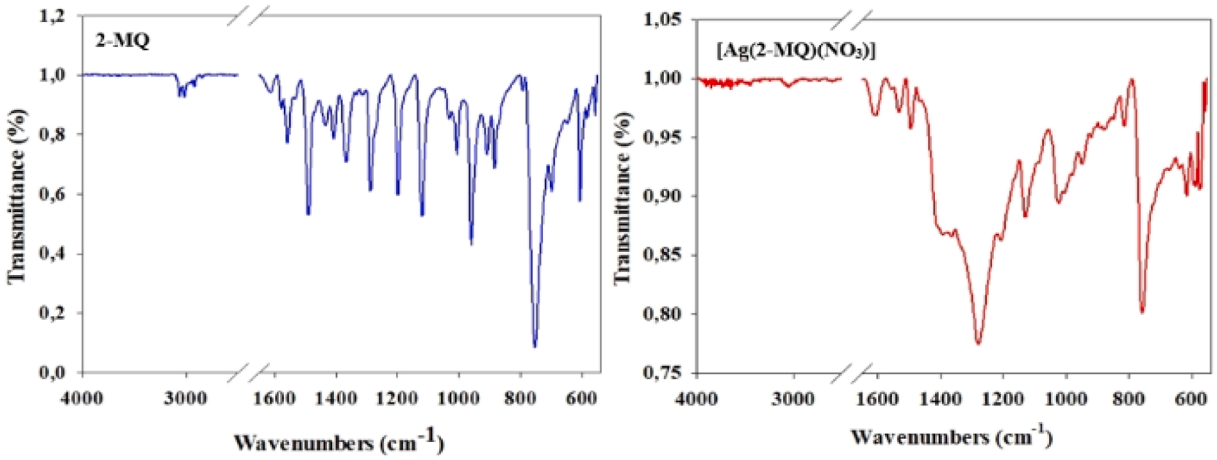

Fig. 4. Experimental FT-IR spectra of 2-MQ and [Ag(2-MQ)(NO_3)].

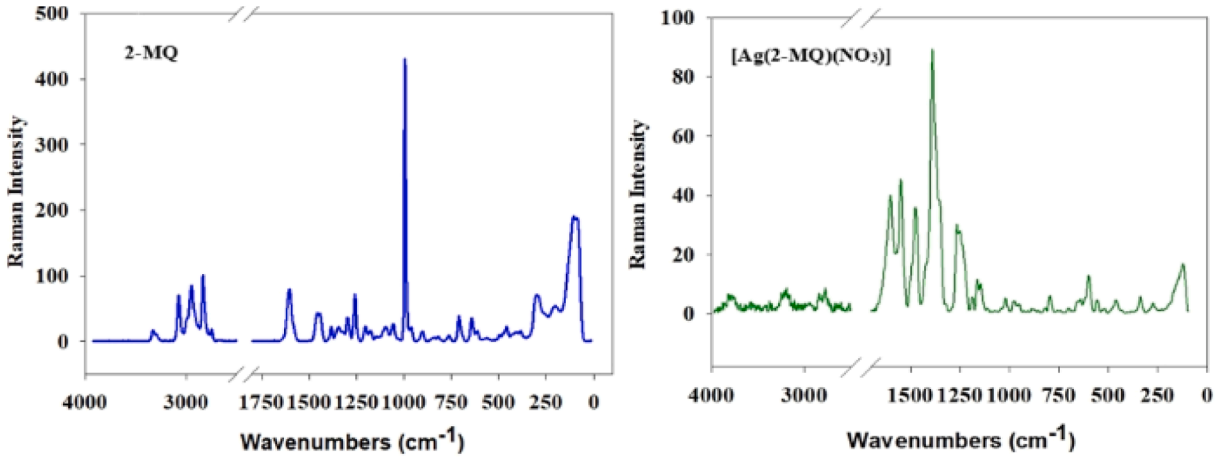

Fig. 5. Experimental FT-Ra spectra of 2-MQ and [Ag(2-MQ)(NO_3)].

stretching modes were measured at 817 cm^{-1} (m, IR) and 801 cm^{-1} (vs, IR), while the [Ag(3-Py-CHO)$_2$NO3] stretching modes were theoretically measured at 840 cm^{-1} [16]. When the Far-IR, FT-IR and FT-Ra spectra of the 2-Methyl-quinoxaline and [Ag(2-MQ)(NO_3)] complex structure are compared, there are new peaks at 1389 (s, IR)/1387 (vs, Ra), 719 (m, IR)/704 (vw, Ra), 643 (vw, IR, Ra), 141 (vw, IR), 124 (w, IR)/ 123 (m, Ra), 100 (w, IR), 80 (m, IR) cm^{-1} in the spectra of the complex structure that are not in the free ligand. These peaks indicate that the complex structure is formed.

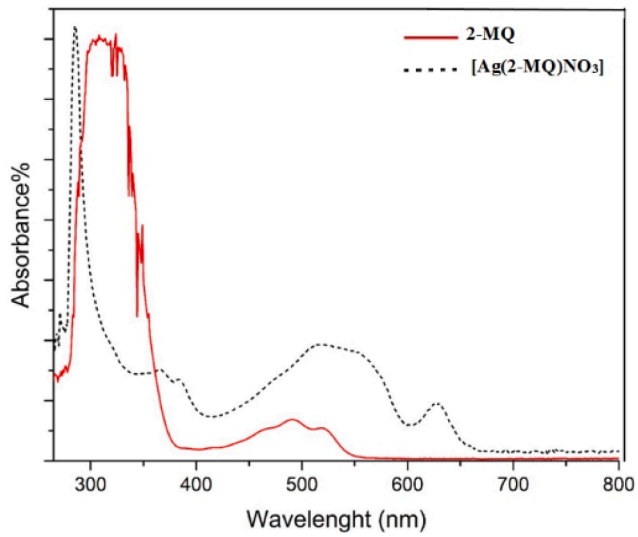

Fig. 6. Experimental UV visible spectra of 2-MQ and [Ag(2-MQ)NO_3].

A linear regression analysis was performed between experimental and theoretical wave numbers. Correlation graphs were drawn and given in supplementary Fig. S1. The equations for 2-MQ and [Ag(2-MQ)(NO_3)] are given below, along with high linear correlation constant (R^2) values.

$$\nu_{cal} = 1.0004\nu_{\exp} - 2.0047 R^2 = 0.9998 for IR of 2-M \quad (1)$$

$$\nu_{cal} = 1\nu_{\exp} - 0.6165 R^2 = 0.9999 for Ramano f 2-MQ \quad (2)$$

$$\nu_{cal} = 1.0005\nu_{\exp} + 3.6944 R^2 = 0.9998 for IR of [Ag(2-MQ)(NO_3)] \quad (3)$$

$$\nu_{cal} = 1.0022\nu_{\exp} - 6.6448 R^2 = 0.9994 for Ramano f [Ag(2-MQ)(NO_3)] \quad (4)$$

According to these R^2 values, there is good agreement between the experimental and calculted frequencies. That is, the experimental IR and Raman bands were highly harmony reproduced by DFT calculations for both the free ligand and the silver nitrate complex [41].

3.3. ^1H NMR analysis

^{1}H NMR spectra were recorded in DMSO solution using a liquid

Table 4
Theoretical calculated wavelengths, excitation energies, oscillator strengths and major contributions in DMSO.

Compound	λ (nm)	E (eV)	f (Hz)	Symmetry	Major Contributioans
2-MQ	185.60	6.68	0.4302	Singlet-A	H-1 → L + 6
	211.46	5.86	0.6631	Singlet-A	H → L + 2
	274.88	4.51	0.1005	Singlet-A	H → L
[Ag(2-MQ) NO_3]	216.56	5.72	0.7042	Singlet-A	H-1 → L + 2
	287.77	4.31	0.1194	Singlet-A	H-1 → L

Bruker 400 MHz AV model NMR spectrometer with an operating frequency of 400 MHz and the spectra are presented in supplementary Fig. S2. In the experimental ^{1}H NMR spectra of the 2-MQ and [Ag(2-MQ)(NO3)] complex, aromatic protons 12H, 13H, 15H, and 16H in the benzene rings were detected at 8.03/7.82, 8.09/8.47, 7.75/7.26, and 7.27/7.12 ppm, respectively. Signals for proton 14H in the pyrazine ring of the free ligand and its silver nitrate complex were observed at 8.75 and 8.17 ppm. Finally, H17, H18, and H19 protons in the methyl groups are detected at 2.85 ppm for 2-MQ and 2.51, 1.92, and 2.51 ppm for [Ag(2-MQ)(NO3)] complex. The recorded ^{1}H NMR spectra can be assigned to the aromatic protons in the 2-MQ free ligand and the [Ag(2-MQ)(NO3)] complex. Therefore, the available spectra support the geometry of both the free ligand and the Ag(I) complex.

3.4. UV–visible spectral analysis

The UV–Vis absorption spectra of free ligand and its silver nitrate complex were recorded in DMSO solvent in the range of 190–1100 nm and were given in Fig. 6. A broad absorption band for 2-MQ shows at 325 nm. This band is shifted to 289 nm as narrow band for the [Ag(2-MQ)(NO_3)] complex. Also, the absorbsion band were measured at 493 nm for free ligand, and this bands were determined at 518 nm for the complex structure. Interestingly, a new band was observed at 613 nm for the complex obtained as a result of 2-MQ and silver nitrate being mixed ($AgNO_3$) together. The theoretical absorbance values were computed by using the TD-DFT/B3LYP method with the 6–311++G(d,p) (for 2-MQ) and LANL2DZ (for [Ag(2-MQ)(NO_3)]) basis sets. The calculated wavelengths, excitation energies, oscillator strengths, and major contributions are listed in Table 4.

From the theoretical calculations, splitting two absorbance peaks were determined at 185 nm and 211 nm in for free ligand, while a single absorbance peak was found at 216.56 nm for the Ag(I) complex. Also, the peak calculated at 274.88 nm for the free ligand was found at 287.77 cm for the complex structure. When the experimental and theoretical data are compared with each other, the absorbance values cannot be found in much harmony. For both structures, absorbance bands were observed in the range of 180–300 nm in theoretical calculations, while absorbance peaks were observed in the range of 280–650 nm in experimental measurements.

3.5. Global molecular reactivity descriptor

The electron donating and receiving ability of a molecule is described using the energy values of the HOMO and LUMO [42]. The energy gap of these molecular orbitals provides important information about the reactivity and stability of a molecule. It plays vital role over the electronic and optical properties, luminescence, photochemical reaction, UV–Vis quantum chemistry, and even determining the pharmaceutical and biological properties of the molecule [43-45]. Besides, frontier molecular orbitals (FMO), which are the most important orbitals in a molecule, determine the way the compound interacts with other species and enable the estimation of the reactive position. Quantum chemical property values of 2-MQ and [Ag(2-MQ)NO_3] were listed in Table 5. The HOMO and LUMO energy values were found to be −6.91 eV and −2.15 eV for 2-MQ, these molecular orbital energy values were

Table 5
HOMO, LUMO energies, and global reactivity descriptors of the ligand and its Ag(I) complex.

Molecular Orbital	Energy (eV)			Energy gap (eV)		Ionization potential (I) (eV)		Electron affinity (A) (eV)		Global hardness (η) (eV)		Electronegativity (χ) (eV)		Chemical potential (μ_c) (eV)		Global softness (σ) $(eV)^{-1}$		Global electrophilicity (ω) (eV)	
	*	**		*	**	*	**	*	**	*	**	*	**	*	**	*	**	*	**
H	−6.91	−6.57	ΔE_{H-L}	4.76	3.17	6.91	6.57	2.15	3.40	2.38	1.58	4.53	4.98	−4.53	−4.98	0.42	0.63	4.32	7.83
L	−2.15	−3.40																	
H-1	−6.96	−7.61	$\Delta E_{H-1-L+1}$	5.94	5.63	6.96	7.61	1.02	1.98	2.97	2.81	3.99	4.79	−3.99	−4.79	0.33	0.35	2.68	4.08
L + 1	−1.02	−1.98																	
H-2	−7.19	−7.63	$\Delta E_{H-2-L+2}$	6.95	6.12	7.19	7.63	0.24	1.51	3.47	3.06	3.71	4.57	−3.71	−4.57	0.29	0.33	1.98	3.42
L + 2	−0.24	−1.51																	

H: HOMO (Highest Occupied Molecular Orbital); L: LUMO (Lowest Unoccupied molecular orbital); eV: electron volt; $(eV)^{-1}$: 1/electron volt.
$I = -E_{HOMO}$;$A = -E_{LUMO}$;$\eta = (-E_{HOMO} + E_{LUMO})/2$;$\chi = -\mu_c$;$\mu_c = (E_{HOMO} + E_{LUMO})/2$;$\mu_c = (E_{HOMO} + E_{LUMO})/2$;$\sigma = 1/2\eta$;$\omega = (\mu_c^2)/2\eta$[49].
*2-MQ.
** [Ag (2-MQ)NO_3].

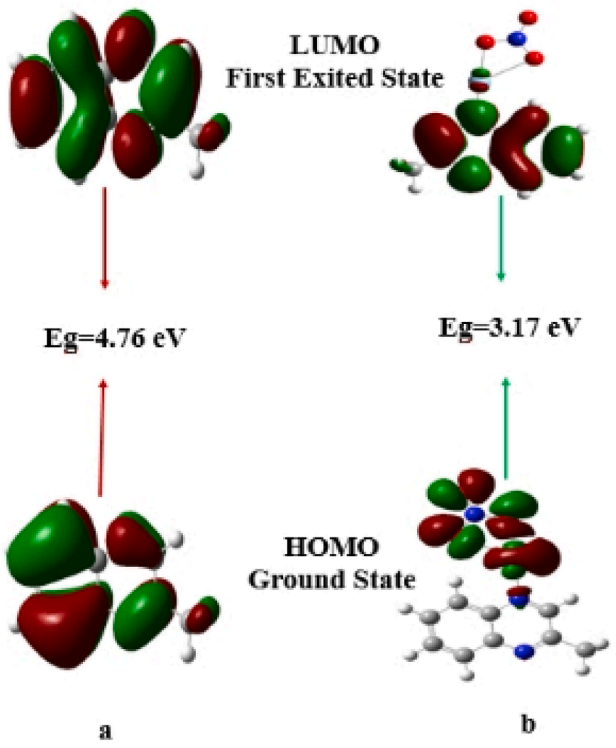

Fig. 7. HOMO-LUMO diagrams of (a) 2-MQ and (b) [Ag(2-MQ)(NO_3)].

found to be.

−6.57 eV and −3.40 eV for the Ag(I) complex. The energy gap values were found to be 4.76 eV and 3.17 eV for both structures. The hardness and softness values of the studied structures are directly related to the energy gap. Hard molecules have a large energy gap. The hardness values were found as 2.38 eV and 1.58 eV for both title structures, respectively. The η value obtained for both structures matches the hard materials in the literature [46,47]. According to HOMO-LUMO energy gap and hardness values, the 2-MQ and Ag(I) complex has low reactivity and this molecule has a hard structure [48]. The LUMO value of this novel synthesized structure was found to be more negative than that of the free ligand, and the HOMO value was also found to be more positive. As a result, the HOMO-LUMO energy gap of the Ag(I) complex structure was found to be smaller, and it was discovered to be more reactive than the free ligand. The HOMO-LUMO distributions of both structures were presented Fig. 7. The HOMO and LUMO distributions for the free ligand were over almost the entire molecule. For the complex, HOMO was distributed over the silver atom and nitrate group while LUMO showed distribution over the ligand.

In Fig. 8, the simulated density state spectrum (DOS), which gives the states of molecular orbitals at different energy levels and helps estimate the optical transition probabilities, is given. The red and green lines in the DOS spectrum allow us to better see virtual orbitals and occupied orbitals, respectively.

3.6. Molecular electrostatic potential (MEP)

The molecular electrostatic potential map is a visual method that provides information on electrophilic and nucleophilic reactivity and hydrogen bonding regions [50]. The red represents the negative electrostatic potential (electrophilic) region, the blue represents the positive (nucleophilic) region, and the green represents the zero potential region. Also, the other colors are intermediate regions [51]. While the negative electrostatic potential regions are expected to be nucleophilic attack regions in this map, the positive electrostatic regions are expected to be electrophilic attack regions [47]. The molecular electrostatic potential (MEP) maps created for free ligand and its Ag(I) complex are given in Fig. 9.

For the 2-MQ, the negative potential regions are concentrated over the N_1 and N_2 atoms in the pyrazine ring. The C atoms in the benzene ring are in the yellow region. In other words, they are in the less electronegative region compared to the atoms in the red region. Also, all of the H atoms of the 2-MQ are in the positive (blue) region. According to the MEP map of the Ag(I) complex it was determined that the regions of negative potential (electrophilic) were changed and localized on the O atoms in the nitrate group. Also, the N_2 atom in the pyrazine ring has become less electronegative than N_2 of the 2-MQ molecule. The Ag and N1 atoms are in the positive blue region in this new compound. Also, all of the H atoms are located in the positive-charged region. In the literatüre, for a nicotinaldehyde silver (I) nitrate complex [Ag(3-Py-CHO)$_2$(NO_3)], electron-rich regions (negative regions) in the MEP map were also distributed over the nitrate group [16].

3.7. Charge analysis

The molecular orbital investigations give important information on the binding potential and reactivity of the molecules. Electronic charges also affect the electronic structure, molecular polarizability, dipole moment, Fukui functions, and other molecular properties [36].

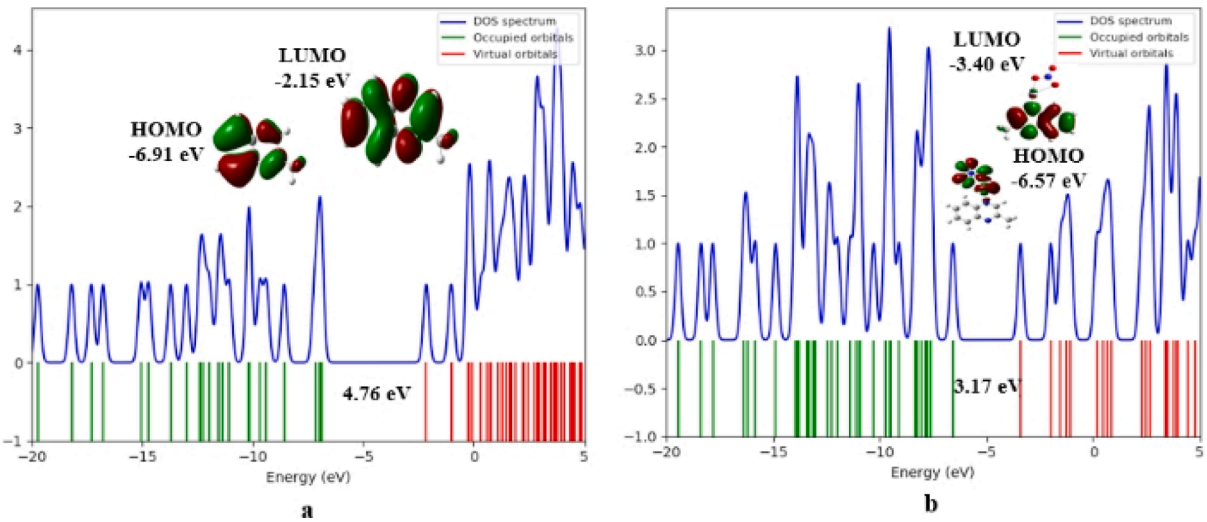

Fig. 8. DOS spectra of (a) 2-MQ and (b) [Ag(2-MQ)NO_3].

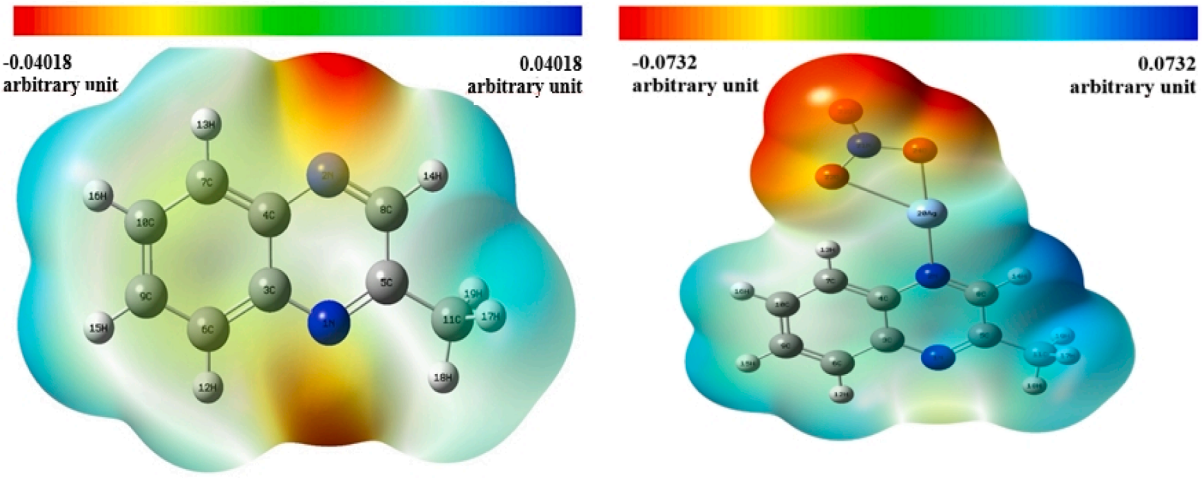

Fig. 9. Molecular electrostatic potential surfaces (MEP) for 2-MQ and [Ag(2-MQ)NO_3].

Table 6
Comparison of NBO, Hirshfeld and APT atomic charges for 2-MQ and [Ag(2-MQ)NO_3].

2-MQ				[Ag(2-MQ)(NO_3)]			
Atoms	APT	Hirshfeld	NBO	Atoms	APT	Hirshfeld	NBO
N_1	−0.306	−0.174	−0.416	N_1	−0.234	−0.173	−0.453
N_2	−0.207	−0.172	−0.389	N_2	−0.163	−0.087	−0.567
C_3	0.099	0.049	0.128	C_3	0.098	0.060	0.163
C_4	0.037	0.046	0.111	C_4	−0.038	0.061	0.169
C_5	0.262	0.071	0.182	C_5	0.228	0.082	0.237
C_6	−0.031	−0.041	−0.178	C_6	−0.057	−0.035	−0.187
C_7	0.004	−0.038	−0.171	C_7	−0.044	−0.033	−0.202
C_8	0.054	0.026	0.023	C_8	−0.008	0.049	0.077
C_9	−0.031	−0.038	−0.192	C_9	0.008	−0.030	−0.189
C_{10}	−0.057	−0.041	−0.197	C_{10}	−0.022	−0.025	−0.178
C_{11}	−0.022	−0.094	−0.604	C_{11}	−0.065	−0.099	−0.664
H_{12}	0.053	0.051	0.216	H_{12}	0.076	0.071	0.242
H_{13}	0.052	0.052	0.217	H_{13}	0.117	0.066	0.249
H_{14}	0.012	0.057	0.194	H_{14}	0.073	0.078	0.226
H_{15}	0.036	0.053	0.211	H_{15}	0.050	0.069	0.232
H_{16}	0.037	0.052	0.208	H_{16}	0.064	0.074	0.238
H_{17}	−0.006	0.046	0.215	H_{17}	0.019	0.057	0.237
H_{18}	0.018	0.048	0.227	H_{18}	0.046	0.062	0.251
H_{19}	−0.006	0.046	0.215	H_{19}	0.019	0.057	0.237
				Ag	0.671	0.196	0.658
				N_{21}	1.269	0.247	0.685
				O_{22}	−0.708	−0.273	−0.516
				O_{23}	−0.664	−0.231	−0.364
				O_{24}	−0.738	−0.243	−0.584

Therefore, it is a very important type of analysis for quantum chemical calculations. The calculated atomic polar tensor (APT), Hirshfeld, and natural bond orbital (NBO) charge values are listed in Table 6 and presented in supplumentary Fig. S3.

According to the APT, Hirsfeld and NBO atomic charge analysis of the 2-MQ, N_1, N_2, C_6, C_9, C_{10}, and C_{11} atoms were found to have negative values. The positive charge values were found over C_3, C_4, C_5, C_8, and most of the H atoms for three charge types. When the molecular electrostatic potential surface map is compared with the atomic charge analysis of free ligand, the electrophilic and nucleophilic regions in the map are in harmony with negative and positive atomic charges.

In the atomic charge analysis of the Ag(I) complex, the most positive charge values were observed on the Ag_{20} and N_{21} atoms. Besides, C_3, C_5, and all H atoms were found to be positive for this complex structure in three charge types. Because O atoms in the nitrate group have a negative charge, the coordination environment around the central metal (Ag) atom has also occurred. Other negative-charged atoms are found as N_1, N_2, C_6, C_7, C_8,C_{10}, and C_{11} atoms in the APT, Hirshfeld, and NBO charge analyses. The molecular electrostatic potential surface map matches the atomic charge analysis of this complex structure for all atoms except N_2 and O.

3.8. Non-covalent interaction

3.8.1. Topological analysis (AIM)

The AIM innovative approach (Atoms in Molecules) [52] invented by R. Bader [53,54] is widely used to determine inter and intra-atomic interaction calculations, the electronic structure, the reactivity, etc. [55]. The topological parameters such as the electron density ρ(r), the Laplacian values $\nabla^2\rho(r)$, the energy density H(r), which makes it possible to evaluate the properties of the bonds in the compound and more particularly the hydrogen bonds. According to Rozas et al. [56], the latter can be divided into three categories:

– Weak hydrogen bonds: $\nabla^2\rho(r) > 0$ and $H(r) > 0$.
– Moderate hydrogen bonds: $\nabla^2\rho(r) > 0$ and $H(r) < 0$.
– Strong or very strong hydrogen bonds: $\nabla^2\rho(r) < 0$ and $H(r) < 0$.

The AIM molecular graph of the ligand and its Ag(I) complex are gathered in Fig. 10 and the topological parameters of non-covalent

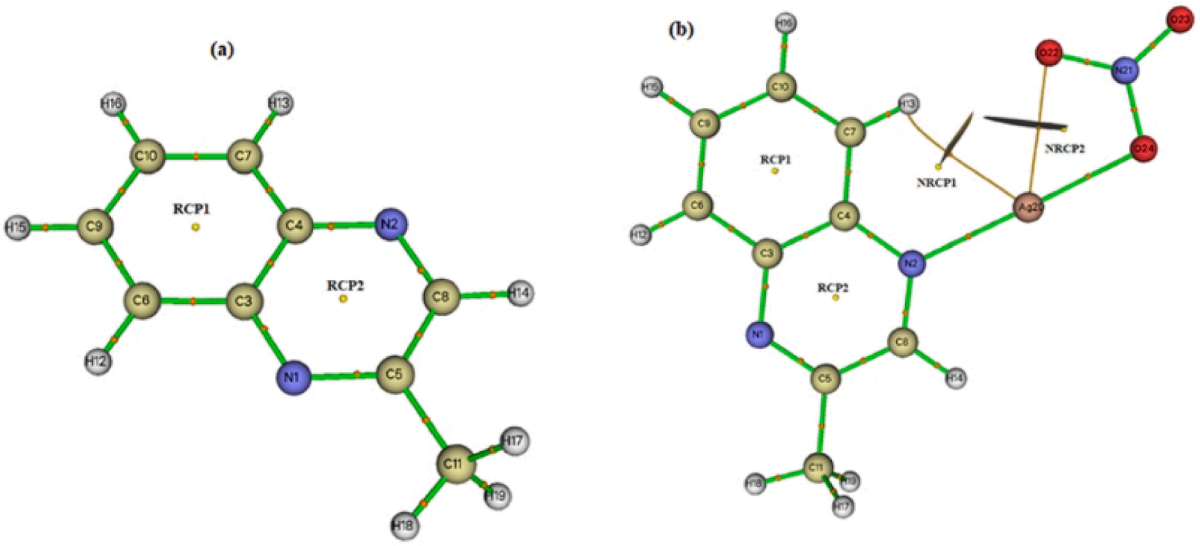

Fig. 10. AIM molecular graphs of ligand (a) and Ag(I) complex (b).

Table 7
Topological parameters for ligand and its Ag(I) complex.

Interactions	ρ(r)	$\nabla^2\rho(r)$	H(r)	G(r)	V(r)	E_{bond}(kJ/mol)	|V(r)|/ G(r)	λ_1	λ_2	λ_3
2-MQ										
RCP1	0.02169	0.15929	0.00755	0.03226	−0.02471	–	0.76	−0.01728	−0.08397	0.09259
RCP2	0.02582	0.18701	0.00796	0.03878	−0.03081	–	0.79	−0.02329	0.10062	0.10968
[Ag(2-MQ)NO_3]										
RCP1	0.02091	0.15129	0.00473	0.03309	−0.02835	–	0.85	−0.01727	−0.08327	0.08529
RCP2	0.02253	0.16664	0.00542	0.03625	−0.03083	–	0.85	−0.01997	0.08484	0.10179
NRCP1	0.02323	0.11379	0.00280	0.02564	−0.02284	–	0.89	−0.98218	−0.92758	0.15929
NRCP2	0.01069	0.04413	0.00194	0.00909	−0.00714	–	0.78	−0.00765	0.00575	0.04603
C_7-H_{13}….Ag	0.01093	0.04155	0.00176	0.00862	−0.00685	8.99	0.79	−0.00873	−0.00412	0.05441
N_{21}-O_{22}….Ag	0.02636	0.11807	0.00158	0.02793	−0.02635	34.58	0.94	−0.02317	−0.02151	0.16277
N_2-Ag	0.07819	0.34817	−0.01731	0.10435	−0.12166	159.68	1.16	−0.09250	−0.08794	0.52837
O_{24}- Ag	0.06909	0.35634	−0.01035	0.09944	−0.10980	144.11	1.10	−0.08779	−0.081004	0.52534

intermolecular interactions were listed in Table 7. The results of the AIM study are crucial not just at H-bond critical points but also for understanding bond critical points (BCPs) and ring critical point (RCPs) properties [57]. According to this analysis, there are two ring critical points RCPs in ligand and new ring critical points NRCPs in its Ag(I) complex. In the ligand and in the complex, the ρ(r) value in the RCP1 of the benzene ring is lower than that of the closed ring pyrazine ring (RCP2). The presence of an NRCP confirms the atomic stitch's cyclic character. All of the associated $\nabla^2\rho(r)$ values are positive, indicating a concentration of charge around this point. As seen, the hydrogen bond C7-H13….Ag has a positive laplacian and a positive total energy density (H(r)), we can conclude in this case, that this hydrogen bond is weak. The Ag-N bond is shorter than the Ag-O bond, as seen in Table 7, and the ρ(r) and bonding energies value in the complex indicates that Ag-N interaction are stronger than Ag-O interactions. For the C–H···Ag interaction, the average ratio of $|v(r)|/g(r)$ is 0.79, which is less than 1.0. Therefore, these interactions are essentially closed shells for the complex model. Furthermore, the average ratio for Ag–N(O) interactions is slightly>1.0. As a result, Ag–N(O) interactions are intermediate character between the closed shell and the typically covalent interaction for the model of the complex.

3.8.2. Reduced gradient of density (RDG)

The reduced density gradient (RDG) are critical properties in supermolecular chemistry, particularly for biological compounds such nucleic acids. Non-covalent bond interactions, such as π-cation, π-π, and electrostatic interactions between distinct entities that make up the crystal package, are investigated using RDG analysis [57-59]. According to the values of sign (λ2)ρ, these spikes are divided into three regions. These regions are identified with different colors to examine interactions within the studied molecular system. The ligand and its silver complex were modified as plots with a number of weak and strong spikes, as seen in Fig. 11. Comprehending the code colors, where blue color corresponds to hydrogen bond creation, green color refers to Van der Waals attraction, and red color relates to steric repulsion interaction, is important for understanding the types of interactions. The elliptic red plate located at the center of the aromatic rings is related to π-π stacking interactions between the pyrazine and benzene rings, but it also has a strong steric effect due to high repulsions. The green colored isosurface is seen between the hydrogen-silver atoms, which indicate the weak H-bond interaction C-H…Ag, which are attributed to the Van der Waals (VDW) interactions in Ag(I) complex. These results are comparable to those obtained using the AIM approach.

3.8.3. Electron localization function (ELF)

Electron localization function analysis is used to show the atomic shell structure, chemical bond classification, and charge-shift bond verification on the molecular surface [59]. Fig. 12(a, b) shows the 2D and 3D shaded surface projection maps of the ELF isosurface for the ligand and its Ag(I) complex. As it is shown, several colors are represented on this surface. The red and orange colors represent strong electronic localization. The blue color circle represents a depletion region between the inner shell and the valence shell. The red color indicates a high probability of strong n-localized electrons, which are

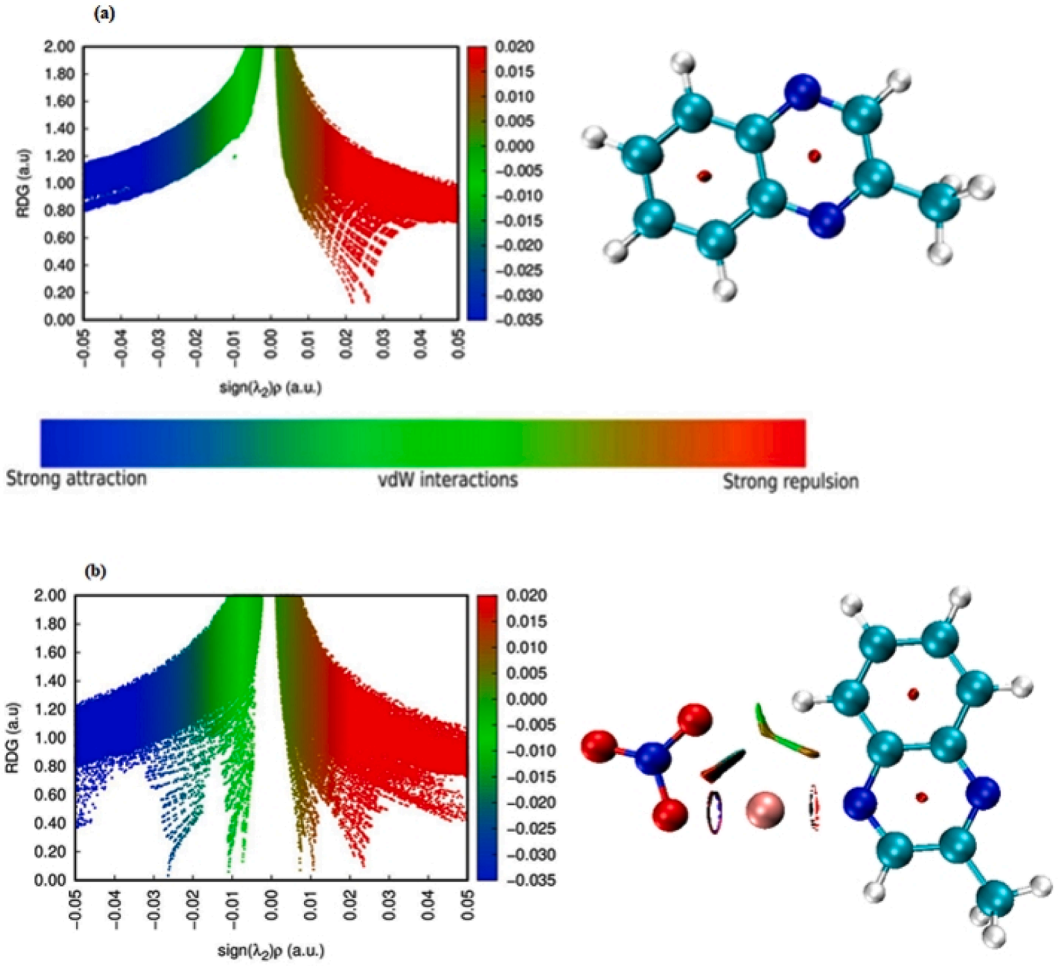

Fig. 11. RDG plot showing non-covalent bond interactions in the ligand (a) and complex (b).

hydrogen atoms, and the blue color indicates a high probability of strongly n-delocalized electrons, which are carbon atoms. The presence of high ELF regions around hydrogen atoms indicates that bonding and non-bonding electrons are highly localized. As shown in Fig. 12(b), electron depletion regions surround the nitrat group in the Ag(I) complex.

3.9. Biological activities

3.9.1. Antimicrobial activity of the parent ligand and its silver complex

2-MQ ligand and [Ag(2-MQ)NO3] complex were tested for antimicrobial activity against a variety of pathogens microbes. As standard reference medications, the antibiotic Ampicillin and the antifungal Nystatin were utilized. The free ligand showed good sensitivity to E. aerogenes and V. anguillarum in the antimicrobial effects test, with inhibition zone values of 12.0 and 30.0 mm inhibition zone widths in both cases (Table 8). Diffusion findings from other agar wells, the highest DIZ of the 2-MQ against C. albicans, B. cereus, S. aureus, E. coli, E. aerogenes, and S. epidermidis was 20, 18, 16, 12, and 12 mm, respectively. In contrast, for the same experiment, L. monocytogenes, E. faecalis, B. subtilis, P. aeruginosa, S. typhimurium, K. pneumoniae, E. coli and S. dysenteria ligand, the lowest DIZ: 10 mm. Antimicrobial testing found that A. hydrophila and C. albicans bacteria and yeast (DIZ: 18 mm) were the most sensitive to the silver complex tested. L. monocytogenes, B. cereus, E. aerogenes, and V. anguillarum were among the bacteria tested, with the lowest DIZ: 15 mm.

By using the agar well diffusion method, the antibacterial activity of Ag(I) complex against V. anguillarum, L. monocytogenes, and B. cereus (DIZ: 15 mm) bacteria was moderately evaluated. The free ligand showed high to moderate antimicrobial activity against bacteria and yeast other than A. hydrophila in the current study. According to the findings, the Ag (I) complex exhibited moderate antimicrobial activity (DIZ: 18 mm) against A. hydrophila, one of the test bacteria used. Table 8 displays the microbial activity results of 2-MQ and [Ag(2-MQ) NO_3 compounds. In this table's MIC (1000 μg/ml) assessment, 2-MQ and [Ag(2-MQ) NO_3] demonstrated good antimicrobial activity against all test bacteria (MIC: 4–128 μg/mL). Our results show that ligand and Ag(I) complex have good a antimicrobial activity against V. anguillarum ATCC 43312, K. pneumoniae ATCC 13883, E. coli ATCC 25922, S. dysenteria ATCC 11835 and C. albicans ATCC 90028 (MIC: 32–128 μg / mL). Bacterial virulence, biofilm formation, and drug resistance are all triggered by the microbial quorum sensing system. Antiquorum sensing can be used to develop a new strategy for preventing microbial resistance [60]. The acyl HSL found in C. violaceum is responsible for the production of violacein, the purple pigment controlled by QS. As a result, drugs that block QS activity in C. violaceum via acyl HSL also block the synthesis of this purple pigment [61]. As a result, the antiquorum-sensing abilities of compounds 2-MQ and [Ag(2-MQ)NO_3] Ag(I) were examined against C. violaceum. Table 8 illustrates the testing findings for their ability to suppress violaceum production mediated by QS against C. violaceum (based on pigment inhibiting diameter in mm), demonstrating that compounds 2-MQ (DIZ: 22 mm) and [Ag(2) -MQ) NO3] (DIZ: 28 mm) have significant antiquorum sensing activity.

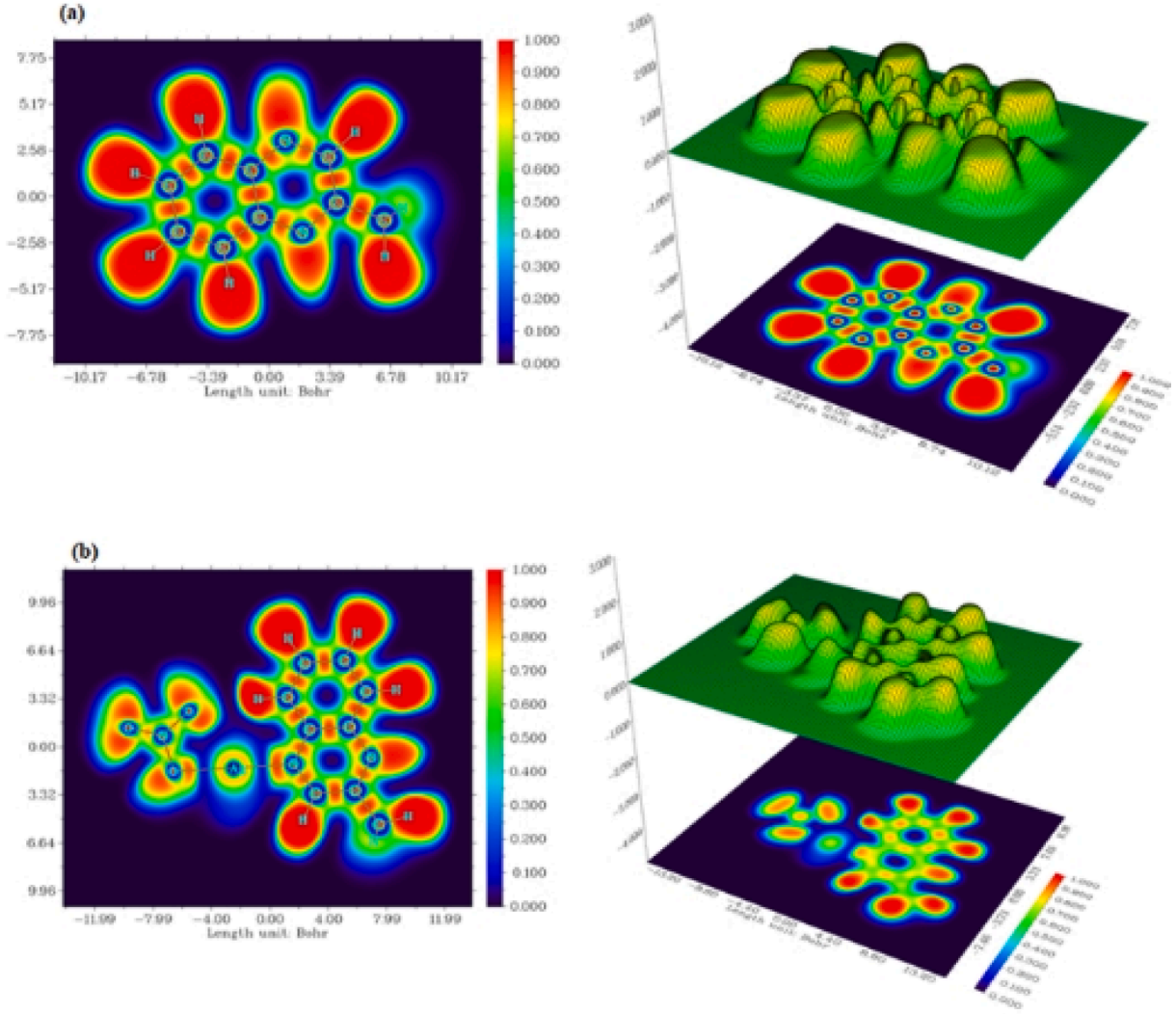

Fig. 12. Colour filled map and 3D surface shaded projection map of ELF for ligand (a) and complex (b).

Table 8
Minimum inhibitory concentration (MIC) and inhibition zone diameter (mm) of 2-MQ and [Ag(2-MQ)NO3] antimicrobial activities.

	2-MQ		[Ag(2-MQ)NO_3]				
Test Bacteria	DIZ (mm)	MIC (μg/ml)	DIZ (mm)	MIC (μg/ml)	AMP (10 μg)	Nystatin (200 μg)	DMSO 10%
S. aureus ATCC 25923	16	16	–	–	na	–	–
S. epidermidis ATCC 35984	12	8	–	–	na	–	–
L.monocytogenesATCC 35152	10	4	15	8	15	–	–
E. faecalis ATCC 29212	10	4	–	–	12	–	–
B. cereus 709 Roma	18	8	15	8	12	–	–
B. subtilis ATCC 6633	10	4	–	–	12	–	–
E. aerogenes ATCC 51342	12	8	15	16	18	–	–
A. hydrophila ATCC 7966	–	–	18	16	18	–	–
P. aeruginosa ATCC 27853	10	16	–	–	16	–	–
V. anguillarum ATCC 43312	30	16	15	8	18	–	–
S.typhimurium ATCC 14028	10	16	–	–	16	–	–
K. pneumoniae ATCC 13883	10	128	–	–	15	–	–
E. coli ATCC 25922	10	32	–	–	15	–	–
S. dysenteria ATCC 11835	10	64	–	–	18	–	–
C. albicans ATCC 90028	20	16	18	16	–	21	–
C. violeceum ATCC 12472 (Antiquorum-sensing activities)	22	64	28	32	nt	–	–

MIC (μg/ml): Minimum Inhibitory Concentration, DIZ (mm): Diameter of inhibition zone (mm),
AMP (10 μg): Ampicillin, nt: not tested, na: no activity, –: no inhibition.

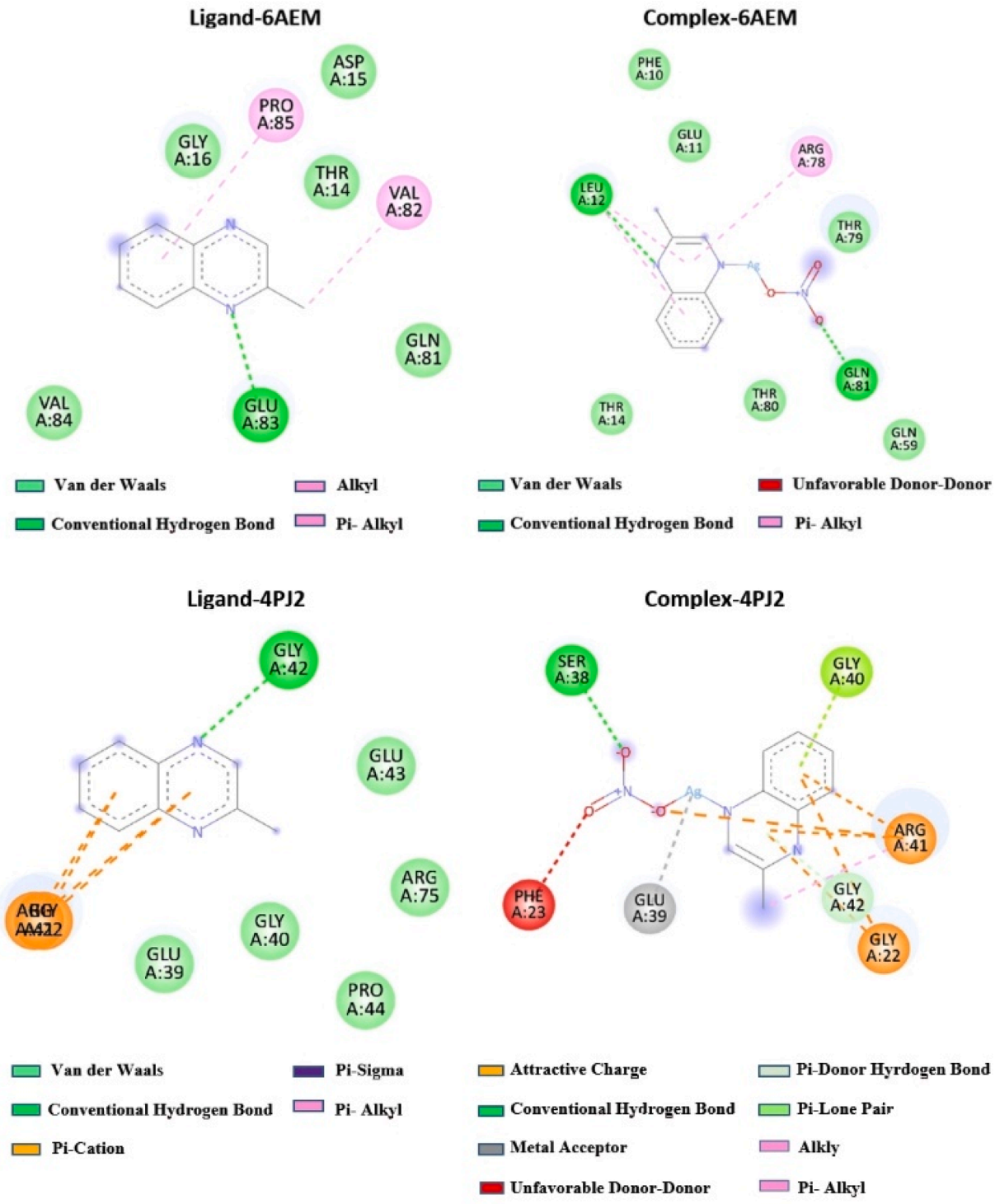

Fig. 13. 2D visual representations of ligand and its Ag(I) complex-antibacterial proteins.

3.9.2. Molecular docking analysis

Molecular docking analysis is a strong theoretical tool for investigating molecular interactions between ligand and protein, which are crucial in biological processes [62-64], such as tumors and bacterial [65,66] diseases. Various antibiotics like echinomycine, levomycin, and actinoleutin contain quinoxaline rings which are used for inhibiting gram +ve bacteria [67]. Many chemical and biological systems contain a high concentration of quinoxaline moiety, which is formed in protein and is active in biological applications [68]. In this study, 2-MQ is a crucial intermediate in the development of biologically active antimicrobial compounds. They are also potent bactericides, thus, molecular docking analysis against the antibacterial proteins were used to assess 2-MQ and its Ag(I) complex's antibacterial activity strain. Many studies have been synthesized and tested as antimicrobial agents of metal complexes of quinoxaline derivatives [6]. In this work, using molecular docking calculations, the antibacterial activity of the studied compounds were compared to the two best bacteria retrieved from the Protein Data Bank (PDB) website (V. anguillarum, PDB: 6AEM, A. hydrophila, PDB: 4PJ2), using molecular docking calculations.

Fig. 13 shows the free 2-MQ ligand and its silver complex 2D binding

Table 9
Docking parameters of ligand and its Ag(I) complex docked with the protein targets.

Receptor	Compound	H-Bonded residues	No of hydrogen bonds	Bonded distance (Å)	Binding Energy (kcal/mol)	Inhibition constant K_i (μM)	Reference RMSD (Å)
6AEM	Ligand	THR 14	3	3.23	−5.69	186.93	24.37
		GLY 16		1.98			
		GLU 83		2.04			
	Complex	LEU 12	3	2.10	−6.80	10.35	33.63
		THR 79		2.39			
		GLN 81		2.23			
4PJ2	Ligand	GLY 42	1	2.19	−5.04	8.50	87.64
	Complex	SER 38	4	2.29	−7.37	3.94	53.48
		SER 38		2.03			
		GLU 39		3.51			
		GLY 42		2.09			

Table 10
Thermodynamic properties at different temperatures of 2-MQ and [Ag(2-MQ)(NO_3)].

T(K)	$C^0_{p,m}$ (J mol^{-1} K^{-1})		S^0_m (J mol^{-1} K^{-1})		ΔH^0_m (kJ mol^{-1})		G_{corr} (kJ mol^{-1})		ε_{ZPE} (kJ mol^{-1})	
	*	**	*	**	*	**	*	**	*	**
100	52.37	110.46	279.05	373.58	1.09	1.93	370.72	410.28	394.04	439.54
200	92.39	164.95	332.67	472.38	2.99	5.41	340.07	367.75	394.04	439.54
300	140.38	223.95	382.46	553.75	5.96	10.25	304.33	316.41	394.04	439.54
400	187.13	279.77	431.77	628.38	10.08	16.47	263.65	257.29	394.04	439.54
500	227.18	326.84	479.83	697.91	15.24	23.94	218.08	190.98	394.04	439.54
600	259.78	368.27	525.75	762.48	21.27	32.41	167.81	117.98	394.04	439.54
700	286.13	394.85	569.13	822.33	28.00	41.69	113.08	38.75	394.04	439.54
800	307.67	419.23	609.90	877.81	35.30	51.62	54.15	−46.23	394.04	439.54
900	325.50	439.22	648.18	929.36	43.06	62.08	−8.73	−136.56	394.04	439.54
1000	340.44	455.81	684.15	977.40	51.22	72.97	−75.32	−231.87	394.04	439.54

*for 2-MQ.
** for [Ag (2-MQ)(NO_3)].
Heat capacit: Entropy: Entalphy changes:Gibbs free energy: Zero point energy.

poses, while Table 9 depicts the different interactions between the investigated compounds and receptors. The binding affinities of the ligand–protein complexes are −5.69 and −5.04 kcal/mol while the interaction energies of the Ag(I) complex with this receptors are −6.80 and −7.37 kcal/mol, respectively. This suggests that the newly synthesized its Ag(I) complex interacts more strongly than the free ligand with the antibacterial proteins. When the electrostatic energy is negative, it indicates that the molecule is bound to a protein [69]. Also given in the table, the inhibition constant (Ki value) is an important parameter to predict whether the synthesized molecule acts as a drug candidate. The Ki value of a drug molecule should not exceed the 10 nanomolar range [70]. According to studies on the interactions between the receptor and the docked compounds, these compounds bind H-bonds with the amino acids within the active site of the receptors. These H-bonds are formed between the nitrogen of the pyrazine ring and the residues. While the free ligand and the 6AEM receptor moieties exhibit interactions with THR'14, GLY'16, and GLU'83, respectively. Similarly, the silver nitrate complex exhibit hydrogen bonds with the macromolecule, the nitrat group forms hydrogen bonds with the –OH and –NH groups of THR'79 and GLN'81 residues with 2.39 Å and 2.23 Å bond distances, respectively. In addition, the nitrogen atom of the pyrazine ring and the nitrogen atom interact with GLY'42 (d = 2.19 Å) for 2-MQ-4PJ2 interaction. The results of docking studies are in good accordance with the results of the non-covalent interactions (NCI) analysis, which is in accordance with the experimental antimicrobial study of title compounds.

3.10. Thermodynamic properties

The thermodynamic properties of materials, which provide important information for technological applications, are closely related to their vibrational properties. For this reason, the entropy, enthalpy change, heat capacity, and change in Gibbs free energy due to the increase in the vibrations of the structures depending on the temperature increase between 100 °K and 1000 °K were investigated. The energy values of the thermodynamic properties at different temperatures are given in Table 10. In addition, the zero point energy values, which are characteristic of the structures, were calculated. The zero point energies for both structures have a constant value at all temperatures, and this value is calculated as 394.04 eV for 2-MQ, while this value is found to be 439.54 eV for the Ag(I) complex structure. Heat capacity, entropy, and enthalpy change values for the free ligand at 100 °K are 52.37, 279.05, and 1.09 kJ/mol, respectively, while these values increase to 340.44, 684.15, and 51.22 kJ/mol at 1000 °K. Similarly, these parameters change for the Ag(I) complex increased with the rise in temperature. As can be seen from the Table 10, the Gibbs free energies for both structures decreased depending on the temperature increase. In the light of all these data, we can say that both structures change their thermodynamic structure depending on the temperature increase.

4. Conclusion

In the present study, we have investigated the theoretical structural, electronic, topological, thermodynamic and vibrational analysis of 2-MQ and its Ag(I) complex computed by DFT methods. AIM, ELF, and RDG approach determine the nature and properties of molecular interactions and reveals clearly the different characteristics of Ag-N and Ag-O bonds. Hence, H-bonds interactions between the C-H…Ag were clearly revealed by AIM studies. TD-DFT has been used to determine the electronic spectrum of title compounds. MEP mapping is determined to predict the nucleophilic and electrophilic reactions of the title compounds. It is seen that the negative potential regions are located on the nitrogen atoms of the pyrazine group for the free ligand, while electron-rich regions for the Ag(I) complex are observed on the nitrate group. The

HOMO-LUMO energy gap values calculated for the complex (3.17 eV) and free ligand (4.76 eV) showed that the structures had bioactivity, while chemical hardness and negative chemical potential provided the stability of the chemicals. According to molecular docking analysis, the newly synthesized Ag(I) complex has significant inhibitory activity for the treatment of antimicrobial diseases. The binding energies of Ag(I) complex against protein receptors 6AEM and 4PJ2 calculated under molecular docking are −6.80 kcal/mol and −7.37 kcal/mol. This work demonstrates a novel application of free ligand and its silver complex for reducing the virulence factors of V. anguillarum, B. cereus, A. hydrophila and C. albicans. This 2-MQ suppresses the QS bacterial system and prevents bacteria and yeast from forming biofilms. Our findings suggest that the 2-MQ and [Ag(2-MQ)(NO_3)] have powerful antimicrobial nosocomial infection control and anti-QS properties, and that the produced title compounds can be employed to treat resistant bacterial infections after additional pharmacological investigations. The antiquorum-sensing activity of the test compounds against C. violaceum ATCC 12472 was investigated, and both the compound ligand and the Ag(I) complex demonstrated good antiquorum-sensing activity.

CRediT authorship contribution statement

Ceyhun Kucuk: . **Senay Yurdakul:** Conceptualization, Data curation, Methodology, Software, Supervision, Validation, Visualization, Writing – original draft. **Sibel Celik:** Conceptualization, Data curation, Investigation, Methodology, Software, Supervision, Validation, Visualization, Writing – original draft. **Belgin Erdem:** Conceptualization, Data curation, Methodology, Validation, Visualization, Writing – original draft.

Declaration of Competing Interest

The authors declare that they have no known competing financial interests or personal relationships that could have appeared to influence the work reported in this paper.

References

[1] J. Yamaguchi, A.D. Yamaguchi, K. Itami, C-H bond functionalization: emerging synthetic tools for natural products and pharmaceuticals, Angew. Chem. Int. Ed. 51 (2012) 8960–9009.

[2] K. Müller, C. Faeh, F. Diederich, Fluorine in pharmaceuticals: looking beyond intuition, Science 317 (2007) 1881–1886.

[3] C. Vaxelaire, P. Winter, M. Christmann, One-pot reactions accelerate the synthesis of active pharmaceutical ingredients, Angew. Chem. Int. Ed. 50 (2011) 3605–3607.

[4] A. Hoffmann-Röder, N. Krause, Synthesis and properties of allenic natural products and pharmaceuticals, Angew. Chem. Int. Ed. 43 (2004) 1196–1216.

[5] T. Tanaka, A. Enomoto, S. Furukawa, K. Fujita, Synthesis of 2-methyl-quinoxaline derivatives from glycerol and diamines catalyzed by iridium complexes bearing an N-heterocyclic carbene ligand, Catalysts. 11 (2021) 1200.

[6] C.W. Kayogolo, M.R. Vegi, B.B.L. Srivastava, M.G. Sahini, Therapeutical potential of metal complexes of quinoxaline derivatives: a review, J. Coord. Chem. 75 (1–2) (2022) 1–48.

[7] T. Kaushal, G. Srivastava, A. Sharma, A.S. Negi, An insight into medicinal chemistry of anticancer quinoxalines, Bioorg. Med. Chem. 27 (2018) 16–35.

[8] V.A. Mamedov, Quinoxalines: Synthesis, Reactions, Mechanisms and Structure, first ed., Springer, Switzerland, 2016, p. 437.

[9] M.M. Alanazi, I.H. Eissa, N.A. Alsaif, A.J. Obaidullah, W.A. Alanazi, A.F. Alasmari, H. Albassam, H. Elkady, A. Elwan, Design, synthesis, docking, ADMET studies, and anticancer evaluation of new 3- methylquinoxaline derivatives as VEGFR-2 inhibitors and apoptosis inducers, J. Enzyme Inhib. Med. Chem. 36 (1) (2021) 1760–1782.

[10] I.A.I. Ali, W. Fathalla, N1 -Allyl-3-substituted-6,7-dimethyl-1, 2-dihydro-2-quinoxalinone as key intermediate for new acyclonucleosides and their regioisomer O-analogues, Heteroat. Chem. 17 (2006) 280–288.

[11] A.J. Barker, E. Hamilton, New hypoxia-selective cytotoxines derived from quinoxaline 1,4-dioxides, J. Heterocycl. Chem. 32 (1995) 1213–1217.

[12] T. Kaushal, G. Srivastava, A. Sharma, A.S. Negi, An insight into medicinal chemistry of anticancer quinoxalines, Bioorg. Med. Chem. 27 (2019) 16–35.

[13] S. Achelle, C. Baudequin, N. Ple, Luminescent materials incorporating pyrazine or quinoxaline moieties, Dyes Pigm. 98 (2013) 575–600.

[14] M. Rizzotto, Metal Complexes as Antimicrobial Agents, Argentina, IntechOpen, 2012, pp. 73–88.

[15] J.R. Allan, A.D. Paton, K. Turvey, Preparation, structural characterisation, and thermal and electrical studies of complexes of zinc, cadmium and mercury with 2-Methyl-quinoxaline, Themochim. Acta 191 (1991) 211–221.

[16] S. Celik, S. Yurdakul, B. Erdem, Synthesis, spectroscopic characterization (FT-IR, PL), DFT calculations and antibacterial activity of silver(I) nitrate complex with nicotinaldehyde, Inorg. Chem. Commun. 131 (2021), 108760.

[17] NCCLS. Performance Standards for Antimicrobial Susceptibility Testing: 10th Informational Supplement (Aerobic Dilution, MIC Testing Supplemental Tables. NCCLS document M100-S10(M7), supplement to NCCLS document M7-A5 (MIC testing), 2000.

[18] NCCLS, Performance Standards for Antimicrobial Susceptibility Testing:13th Informational Supplement (Disk Diffusion Supplemental Tables). NCCLS document M100-S13 (M2), supplement to NCCLS document M2-A8 (disk diffusion), 2003.

[19] M.J. Frisch, G.W. Trucks, H.B. Schlegel, G.E. Scuseria, M.A. Robb, J.R. Cheeseman, G. Scalmani, V. Barone, B. Mennucci, G.A. Petersson, H. Nakatsuji, M. Caricato, X. Li, H.P. Hratchian, A.F. Izmaylov, J. Bloino, G. Zheng, J.L. Sonnenberg, M. Hada, M. Ehara, K. Toyota, R. Fukuda, J. Hasegawa, M. Ishida, T. Nakajima, Y. Honda, O. Kitao, H. Nakai, T. Vreven, J.A. Montgomery, Jr., J.E. Peralta, F. Ogliaro, M. Bearpark, J.J. Heyd, E. Brothers, K.N. Kudin, V.N. Staroverov, R. Kobayashi, J. Normand, K. Raghavachari, A. Rendell, J.C. Burant, S.S. Iyengar, J. Tomasi, M. Cossi, N. Rega, J.M. Millam, M. Klene, J.E. Knox, J.B. Cross, V. Bakken, C. Adamo, J. Jaramillo, R. Gomperts, R.E. Stratmann, O. Yazyev, A.J. Austin, R. Cammi, C. Pomelli, J.W. Ochterski, R.L. Martin, K. Morokuma, V.G. Zakrzewski, G.A. Voth, P. Salvador, J.J. Dannenberg, S. Dapprich, A.D. Daniels, O. Farkas, J.B. Foresman, J. V. Ortiz, J. Cioslowski, D.J. Fox, Gaussian, Inc., Wallingford CT, 2009.

[20] J.J. Kores, I.A. Danish, T. Sasitha, J.G. Stuart, E.J. Pushpam, J.W. Jebaraj, Spectral, NBO, NLO, NCI, aromaticity and charge transfer analyses of anthracene-9,10-dicarboxaldehyde by DFT, Heliyon 7 (2021), e08377.

[21] A. Abdou, H.M. Mostafa, A.M.M. Abdel-Mawgoud, Seven metal-based bi-dentate NO azocoumarine complexes: synthesis, characterization, DFT calculations, Drug-Likeness, in vitro antimicrobial screening and molecular docking analysis, Inorg. Chim. Acta 539 (2022), 121043.

[22] R. Dennington, T. Keith, J. Millam, GaussView, Version 5, Semichem Inc., Shawnee Mission, KS, 2009.

[23] T. Lu, F. Chen, Multiwfn: a multifunctional wavefunction analyzer, J. Comput. Chem. 33 (2012) 580–592.

[24] W. Humphrey, A. Dalke, K. Schulten, VMD: visual molecular dynamics, J. Mol. Graph. 14 (1996) 33–38.

[25] G.M. Morris, D.S. Goodwill, R.S. Halliday, R. Huey, W. Hart, R.K. Belew, A. J. Olson, Automated docking using a Lamarckian genetic algorithm and an empirical binding free energy function, J. Comput. Chem. 19 (1998) 1639–1662.

[26] A. Abdou, A.M.M. Abdel-Mawgoud, Synthesis, structural elucidation, and density functional theory investigation of new mononuclear Fe(III), Ni(II), and Cu(II) mixed-ligand complexes: Biological and catalase mimicking activity exploration, Appl. Organomet. Chem. 36 (4) (2022), e6600.

[27] Biovia Visualization. https://www.3ds.com/products-services/biovia/products/molecular-modeling-simulation/biovia-discovery-studio/visualization/. (accessed 01 March 2022).

[28] A. Thiruvalluar, M. Subramanyam, R.J. Butcher, A.V. Adhikari, S. Wagle, 2-Chloro-3-methylquinoxaline, Acta Crystallogr. E: Crystallogr. Commun. 63 (2007), o4534.

[29] S.S.S. Raj, H.K. Fun, X.F. Chen, X.H. Zhu, X.Z. You, [2-(2-Pyridyl-N)quinoxaline-N1]silver(I) nitrate, Acta Crystallogr. C 55 (1999) 2035–2037.

[30] M. Govindarajan, K. Ganasan, S. Periandy, M. Karabacak, S. Mohan, Vibrational spectroscopic analysis of 2-chlorotoluene and 2-bromotoluene: a combined experimental and theoretical study, Spectrochim. Acta A: Mol. Biomol Spectrosc. 77 (2010) 1005–1013.

[31] H. Gökce, S. Bahçeli, Quantum chemical computations of 1,3-phenylenediacetic acid, Spectrochim. Acta A: Mol. Biomol Spectrosc. 78 (2011) 803–808.

[32] R.M. Ferreiraa, M. Mottaa, A. Batagin-Netoa, C.F.O. Graeffc, P.N. Lisboa-Filhoc, F. C. Lavardac, Theoretical investigation of geometric configurations and vibrational spectra in citric acid complexes, Mater. Res. 17 (3) (2014) 550–556.

[33] Y. Erdogdu, D. Manimaran, M.T. Güllüoglu, M. Amalanathan, I.H. Joeb, S. Yurdakul, FT-IR, FT-Raman, NMR Spectra and DFT Simulations of 4-(4-Fluorophenyl)-1H-imidazole, Opt. Spect. 114 (4) (2013) 525–536.

[34] E.K. Sarıkaya, O. Dereli, Molecular structure and vibrational spectra of 7-Methoxy-4-methylcoumarin by density functional method, J. Mol. Struct. 1052 (2013) 214–220.

[35] N. Prabavathi, A. Nilüfer, V. Krishnakumar, Quantum mechanical study of the structure and spectroscopic (FT-IR, FT-Raman, 13C, 1H and UV), NBO and HOMO–LUMO analysis of 2-quinoxaline carboxylic acid, Spectrochim. Acta A Mol. Biomol. Spectrosc. 92 (2012) 325–335.

[36] S. Murugavel, V.V. Velan, D. Kannan, M. Bakthadoss, Synthesis, crystal structure analysis, spectral investigations, DFT computations, Biological activities and molecular docking of methyl(2E)-2-{[N-(2formlyphenyl)(4-metylbrnzene) sulfonamido]metyl}-3-(4-lurophenyl)prop-2enoate a potential bioactive agent, J. Mol. Struct. 1108 (2016) 150–167.

[37] S. Çelik, M. Alp, S. Yurdakul, A combined experimental and theoretical study on vibrational spectra of 3-pyridyl methyl ketone, Spectrosc. Lett. 53 (4) (2020) 234–248.

[38] S. Srivastava, P. Gupta, A. Sethi, S.R. Pratap, One pot synthesis of Curcumin-NSAIDs prodrug, spectroscopic characterization, conformational analysis, chemical reactivity, intramolecular interactions and first order hyperpolarizability by DFT method, J. Mol. Struct. 1117 (2016) 173–180.

[39] S. Bayarı, A. Ataç, S. Yurdakul, Coordination behaviour of nicotinamide: an infrared spectroscopic study, J. Mol. Struct. 655 (2003) 163–170.

[40] M.T. Bilkan, S. Yurdakul, Z. Demircioğlu, O. Büyükgüngör, Crystal structure, FT-IR, FT-Raman and DFT studies on a novel compound $[C_{10}H_9N_3]AgNO_3$, J. Organomet. Chem. 805 (2016) 108–116.
[41] A. Abdou, O.A. Omran, A. Nafady, I.S. Antipin, Structural, spectroscopic, FMOs, and non-linear optical properties exploration of three thiacaix(4)arenes derivatives, Arab. J. Chem. 15 (3) (2022), 103656.
[42] S. Kumar, V. Saini, I.K. Maurya, J. Sindhu, M. Kumari, R. Kataria, V. Kumar, Design, synthesis, DFT, docking studies and ADME prediction of some new coumarinyl linked pyrazolylthiazoles: potential standalone or adjuvant antimicrobial agents, Ploes One 13 (4) (2018) 0196016.
[43] Z. Demircioglu, C.A. Kastas, O. Büyükgüngör, The spectroscopic (FT-IR, UV-Vis), Fukui Function, NLO, NBO, NPA and Tautomerism Effect Analysis of (E)-2-[(2-hydroxy-6- methoxybenzylidene)amino]benzonitrile, Spectrochim. Acta. A. 139 (2015) 539–548.
[44] H. Ebrahimi, J.S. Hadi, H.S. Al-Ansari, A new series of schiff bases derived from sulfa drugs and indole-3-carboxaldehyde: synthesis, characterization, spectral and DFT computational studies, J. Mol. Struct. 1039 (2013) 37–45.
[45] M.A. Mumit, T.K. Pal, M.A. Alam, M.A.A.A. Islam, S. Paul, M.C. Sheikh, DFT studies on vibrational and electronic spectra, HOMO–LUMO, MEP, HOMA, NBO and molecular docking analysis of benzyl-3N-(2,4,5-trimethoxyphenylmethylene) hydrazinecarbodithioate, J. Mol. Struct. 1220 (2020), 128715.
[46] H. Vural, M. Orbay, Synthesis, crystal structure, spectroscopic investigations and DFT calculations of the copper(II) complex of 4-(Trifluoromethyl)pyridine-2-carboxylic acid, J. Mol. Struct. 1146 (2017) 669–676.
[47] S. Kumar, A. Radha, M. Kour, R. Kumar, A. Chouaih, S.K. Pandey, DFT studies of disubstituted diphenyldithiophosphates of nickel(II): structural and some spectral parameters, J. Mol. Struct. 1185 (2019) 212–218.
[48] S.D. Oladipo, G.F. Tolufashe, C. Mocktar, B. Omondi, Ag(I) symmetrical N, N′-diarylformamidine dithiocarbamate PPh3 complexes: synthesis, structural characterization, quantum chemical calculations and in vitro biological studies, Inorg. Chim. Acta 520 (2021), 120316.
[49] M. Ismael, A. Abdou, A.M. Abdel-Mawgoud, Synthesis, characterization, modeling, and antimicrobial activity of FeIII, CoII, NiII, CuII, and ZnII complexes based on tri-substituted imidazole ligand, Z. Anorg. Allg. Chem. 644 (2018) 1203–1214.
[50] R.R. Saravanan, S. Seshadri, S. Gunasekaran, R.M. Mendoza, S.G. Granda, Conformational analysis, X-ray crystallographic, FT-IR, FT-Raman, DFT, MEP and molecular docking studies on 1-(1-(3-methoxyphenyl) ethylidene) thiosemicarbazide, Spectrochim. Acta. A. Mol. Biomol. Spect. 139 (2015) 321–328.
[51] R.T. Ulahannan, V. Kannan, V. Vidya, K. Sreekumar, Synthesis and DFT studies of the structure - NLO activity evaluation of 2-(4-methoxyphenyl)-1,4,5-triphenyl-2,5-dihydro-1H-imidazole, J. Mol. Struc. 1199 (127004) (2020) 1–7.
[52] P.L.A. Popelier, F.M. Aicken, S.E. O'Brien, Atoms in molecules, an introduction, Prentice Hall (2000) 143–198.
[53] R.F.W. Bader, M.A. Austen, Properties of atoms in molecules: atoms under pressure, J. Chem. Phys. 107 (1997) 4271–4285.
[54] R.F.W. Bader, Atoms in Molecules: A. Quantum Theory, Oxford Univ. Press, 1990, 2.
[55] M. Harzallah, M. Medimagh, N. Issaoui, T. Roisnel, A. Brahim, Synthesis, X-ray crystal structure, Hirshfeld surface analysis, DFT, AIM, ELF, RDG and molecular docking studies of bis[4-(dimethylamino)pyridinium]di-μ-chloridobis [dichloridomercurate(II)], J. Coord. Chem. 74 (17–20) (2021) 2927–2946.
[56] I. Rozas, I. Alkorta, J. Elguero, Behavior of ylides containing N, O, and C atoms as hydrogen bond acceptors, J. Am. Chem. Soc. 122 (45) (2000) 11154–11161.
[57] O. Noureddine, S. Gatfaoui, S.A. Brandan, H. Marouani, N. Issaoui, Structural, docking and spectroscopic studies of a new piperazine derivative, 1-Phenylpiperazine-1,4-diium bis(hydrogen sulfate), J. Mol. Struc. 1202 (2020), 127351.
[58] T.B. Issa, A. Sagaama, N. Issaoui, Computational study of 3-thiophene acetic acid: molecular docking, electronic and intermolecular interactions investigations, Comput. Biol. Chem. 86 (2020), 107268.
[59] Y. Sheena Mary, Y. Shyma Mary, A.S. Rad, R. Yadav, I. Celik, S. Sarala, Theoretical investigation on the reactive and interaction properties of sorafenib – DFT, AIM, spectroscopic and Hirshfeld analysis, docking and dynamics simulation, J. Mol. Liq. 330 (2021), 115652.
[60] X. Zhao, Z. Yu, T. Ding, Quorum-sensing regulation of antimicrobial resistance in bacteria, Microorganisms 8 (3) (2020) 425.
[61] W. Chu, D.A. Vattem, V. Maitin, M.B. Barnes, R.J. McLean, Bioassays of quorum sensing compounds using Agrobacterium tumefaciens and Chromobacterium violaceum, Methods Mol. Biol. 692 (2011) 3–19.
[62] R. Maheswari, J. Manjula, Vibrational spectroscopic analysis and molecular docking studies of (E)-4-methoxy-N0 -(4-methylbenzylidene) benzohydrazide by DFT, J. Mol. Struct. 1115 (2016) 144–155.
[63] H.M. Patel, D.P. Rajani, M.G. Sharma, Synthesis, molecular docking and biological evaluation of mannich products based on thiophene nucleus using ionic liquid, Lett. Drug Des. Discov. 16 (2019) 119–126.
[64] M.H. Patel, K.D. Patel, H.D. Patel, Facile synthesis and biological evaluation of New Mannich products as potential antibacterial, antifungal and antituberculosis agents: molecular docking study, Curr. Bioact. Compd. 13 (2017) 47–58.
[65] S. Mondal, S.M. Mandal, T.K. Mondal, Spectroscopic characterization, antimicrobial activity, DFT computation and docking studies of sulfonamide Schiff bases, J. Mol. Struct. 1127 (2017) 557–567.
[66] S. Mondal, S.M. Mandal, T.K. Mondal, Structural characterization of new Schiff bases of sulfamethoxazole and sulfathiazole, their antibacterial activity and docking computation with DHPS protein structure, Spectrochim. Acta Mol. Biomol Spectrosc. 150 (2015) 268–279.
[67] V. Desai, S. Desai, S.N. Gaonkar, U. Palyekar, S.D. Joshi, S.K. Dixit, Novel quinoxalinyl chalcone hybrid scaffolds as enoyl ACP reductase inhibitors: synthesis, molecular docking and biological evaluation, Bioorg. Med. Chem. Lett. 27 (10) (2017) 2174–2180.
[68] R.R. Varma, J.G. Pandya, F.U. Vaidya, C. Pathak, R.A. Dabhi, M.P. Dhaduk, B. S. Bhatt, M.N. Patel, DNA interaction, anticancer, antibacterial, ROS and lipid peroxidation studies of quinoxaline based organometallic Re(I) carbonyls, J. Mol. Struct. 1240 (2021), 130529.
[69] A. Üngördü, N. Tezer, Effect on frontier molecular orbitals of substituents in 5-position of uracil base pairs in vacuum and water, J. Theor. Comput. Chem. 16 (07) (2017) 1750066.
[70] N. Nagasundaram, K. Padmasree, S. Santhosh, N. Vinoth, N. Sedhu, A. Lalitha, Ultrasound promoted synthesis of new azo fused dihydropyrano[2,3-c]pyrazole derivatives: In vitro antimicrobial, anticancer, DFT, in silico ADMET and Molecular docking studies, J. Mol. Struct. 1263 (2022), 133091.